

**OPTIMIZATION OF TRANSVERSE RESISTIVITY FOR
INCREASED STABILITY IN RAMPED CABLE-IN-CONDUIT
SUPERCONDUCTING MAGNETS**

by

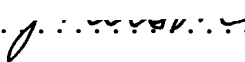
Richard J. Nelson

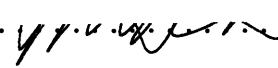
B.S., Applied Physics
Brigham Young University, 1992


Submitted to the Department of Mechanical Engineering
in Partial Fulfillment of the Requirements for the Degree of

Master of Science in Mechanical Engineering

at the
Massachusetts Institute of Technology
February 1995

Author 
Richard J. Nelson
Department of Mechanical Engineering
February 10, 1995

Certified by 
Yukikazu Iwasa
Research Professor, Francis Bitter National Magnet Laboratory
Senior Research Engineer, Department of Mechanical Engineering
Thesis Advisor

Accepted by 
Ain A. Sonin
Chairman, Graduate Committee
Department of Mechanical Engineering

1 Eng.

MASSACHUSETTS INSTITUTE
OF TECHNOLOGY

APR 06 1995

LIBRARIES

© 1995 Richard J. Nelson. All rights reserved.

The author hereby grants to MIT permission to reproduce and to distribute publicly paper and electronic copies of this thesis document in whole or in part.

Optimization of Transverse Resistivity for
Increased Stability in Ramped Cable-in-Conduit
Superconducting Magnets

by

Richard J. Nelson

Submitted to the Department of Mechanical Engineering on February 10, 1995,
in partial fulfillment of the requirements for the Degree of
Master of Science in Mechanical Engineering

ABSTRACT

Three experiments to determine the stability of a cable-in-conduit (CIC) conductor under ramping conditions were performed on a Nb₃Sn sub-size model coil of magnets intended for use as the central solenoid coil for the International Thermonuclear Experimental Reactor (ITER). The CIC conductor is a 48-strand cable, each strand coated with 2 μm thick chromium. The first experiment determined the time constant for coupling currents between strands through AC loss measurements. The second experiment measured the stability margin of the model coil against short length disturbances. The final experiment recorded the "ramp rate limitation" due to a transport current ramp. Analysis of the results of all three experiments suggest that it may be possible to maximize the stability margin of a ramping magnet by optimizing the insulating coating thickness; subsequently, a plan to determine the optimum thickness is formulated.

The results of the AC loss experiment indicate good agreement between experiment and theory for coupling in a homogeneous mixture, thus validating the inverse relationship between coupling loss and effective transverse resistivity. The stability experiment revealed a limiting current well below the theoretical value predicted by the Stekly formula; however, the ill-cooled and well-cooled regimes are clearly present. The experiment on the ramp rate limitation showed little degradation in maximum attainable quench current under fast current ramps; since the maximum self-field ramp rate was only 0.05 T/s during the fastest current ramp, the limitation seen in other magnets is likely due to fast magnetic field ramps.

It is hypothesized that the thermal stability margin at constant operating current is valid for ramping conditions as well, and that the ramp rate limitation is due to the electromagnetic response to a current maldistribution among the strands. It is then proposed that the AC loss and ramp rate limitation phenomena be treated as mathematically independent. Finally, a procedure for determining the optimum electrical insulation thickness for the strands is suggested that balances the AC losses and the ramp-rate limitation.

Thesis supervisor: Dr. Yukikazu Iwasa

ACKNOWLEDGMENTS

I would like to first thank my wife, Elizabeth, who unselfishly followed me around the globe from Boston to Japan so that I could enrich my educational experience. Gratitude is due my thesis advisor, Dr. Yukikazu Iwasa, who first introduced me to superconducting magnet technology, and from whom I have learned far more than any course on the subject could teach. Many thanks are due to Dr. Yoshikazu Takahashi, who mentored the experiments on which this thesis is based; further thanks are also in order for the rest of my friends at the Superconducting Lab of the Japan Atomic Energy Research Institute, who not only pivotally contributed to my understanding of the ITER project, but also advanced significantly my understanding and enjoyment of another culture. Finally, I immensely appreciate the support of my family, especially my brother Kevin, who spent with me many enervating evenings by phone so that I might maintain my sanity at graduate school; and my mother, Jody, who instilled in me a passion for the pursuit of knowledge; and most particularly my father, Richard E. Nelson, who never refused to believe that I could accomplish whatever ambitious project I might choose to undertake.

The experimental portion of this thesis was performed at the Japan Atomic Energy Research Institute in Naka-machi, Japan, with generous support from a Starr Foundation fellowship. The author thanks the Starr Foundation and the MIT-Japan program for making the experience abroad possible and productive.

This research was supported in part by the Office of Fusion Energy, United States Department of Energy. The author appreciates the generous backing of this department for having established a positive US-Japan collaboration and supporting this work from beginning to end.

This material is based upon work supported under a National Science Foundation Graduate Research Fellowship. Any opinions, findings, conclusions or recommendations expressed in this publication are those of the author and do not necessarily reflect the views of the National Science Foundation.

TABLE OF CONTENTS

Chapter 1. Introduction	10
1.1 Overview	10
1.2 Background	13
1.2.1 Properties of Superconducting Materials	13
1.2.2 Superconducting Strands	15
1.2.3 Cable in Conduit Conductors	16
1.2.4 AC Losses	17
1.2.5 Stability	18
1.2.6 Ramp Rate Limitation	19
1.3 Sample Conductor	20
Chapter 2. AC Loss Experiment	22
2.1 Overview	22
2.2 Theoretical Background	22
2.3 Experimental Procedure and Analysis	26
2.3.1 Determining Hysteresis Loss	26
2.3.2 Determining Coupling Loss	27
2.4 Results and Discussion	28
Chapter 3. Stability Experiment	30
3.1 Overview	30
3.2 Theoretical Background	31
3.3 Experimental Procedure	34
3.4 Analysis and Results	35
3.5 Discussion	38
Chapter 4. Ramp Rate Limitation Experiment	40
4.1 Overview	40
4.2 Theoretical Background	40
4.3 Experimental Procedure	43
4.4 Analysis and Discussion	43
Chapter 5. General Discussion and Recommendations	45
5.1 Maximizing Magnet Stability Using Transverse Resistance	45
5.1.1 Determination of Anticipated AC Losses	47
5.1.2 Stability Against AC Losses	48
5.1.3 Stability with Ramp Rate Limitation Phenomenon	49
5.1.4 Controlling Effective Transverse Resistance	52
5.2 Conclusion	53
Bibliography	56

LIST OF FIGURES

1.1	Schematic drawing showing two principal coils (and fields) in a tokamak. The toroidal field provides B_ϕ for plasma stability, while the poloidal coil in the center provides B_z for plasma heating. (from M. N. Wilson, <i>Superconducting Magnets</i> , Clarendon Press: Oxford, 1983)	10
1.2	Cross section of a typical cable-in-conduit (CIC) conductor. This conductor has 48 strands: three wires twisted in triplets, then four triplets twisted in a group, and finally four groups twisted together and compacted inside the conduit. (from R. J. Nelson, "An Investigation of A.C. Losses in Two Sub-size Conductors for the ITER," JAERI-M 93-219: 1993)	12
1.3	The critical surface of a typical engineering grade superconductor in temperature-current density-magnetic field space. States below the critical surface are superconducting, while states above the surface are "normal," or resistive. (from Y. Iwasa, <i>Case Studies in Superconducting Magnets: Design and Operational Issues</i> , Plenum Press: New York, 1994)	14
1.4	A single 0.92-mm diameter strand of a typical Nb_3Sn conductor, containing 22,591 Nb_3Sn filaments, with some niobium and bronze, surrounded by a tantalum barrier and a copper stabilizer. A layer of chromium insulation 2 μm thick coats the surface. (from R. J. Nelson, "An Investigation of A.C. Losses in Two Sub-size Conductors for the ITER," JAERI-M 93-219: 1993)	16
1.5	Ramp rate limitation results in the DPC-EX coil when both current and background field are ramped at a constant rate. Solid circles represent quench currents, while open circles represent stable currents. (from M. Nishi <i>et. al.</i> , "Ramp-Rate Limitation Test Results of the Nb_3Sn Demo Poloidal Coil (DPC-EX)," presented at the 15th Symposium on Fusion Engineering: Hyannis, Massachusetts, October 11-15, 1993)	19
1.6	Diagram of the sample coil, used for the experiments in this thesis. The coil was wound with the CIC conductor whose cross section is pictured in Fig. 1.2. The 10-turn sample coil has a total length of 6.3 m. Other relevant parameters are noted in Table 1.1.	21
2.1	A schematic representation of the experimental setup for hysteresis loss and coupling loss measurements. From these two measurements the coupling time constant (τ_{cpl}) was determined.	22

2.2	Cross-sectional cut showing the relative locations of the experimental coil and pick-up coils for the experiment. Not to scale.	26
2.3	The hysteresis curve for the sample The area inside the curve represents the hysteresis loss as the external field goes from zero to 1.15 T and back to zero.	27
2.4	The coupling loss during an exponential dump of the background field, plotted versus the inverse of the background field decay constant. The curves, based on Eq. 2.11, show a coupling time constant (τ_{cpl}) of about 27 ms for this sample.	28
3.1	A schematic showing the experimental setup for the stability and the ramp rate experiments.	30
3.2	The stability margin plotted versus operating current for an inductive heating length of 50 mm. Open circles represent stability after energy deposition; solid circles represent magnet quench. The solid triangle indicates a quench initiated far downstream from the heated region.	36
3.3	The stability margin plotted versus operating current for an inductive heating length of 200 mm. Open circles represent stability after energy deposition; solid circles represent magnet quench. The solid triangle indicates a quench initiated far downstream from the heated region.	37
3.4	A typical recording of the voltage rise caused by superconducting-to-normal transition during a quench. The trace marked V5-V7 corresponds to the voltage difference between voltage taps placed 317 cm apart; the trace marked V7-V9 recorded the voltage difference between voltage taps placed 162 cm apart.. . . .	38
4.1	Schematic representation of the ramp rate limitation model proposed by Takayasu (from M. Takayasu <i>et. al.</i> , "Measurements of Ramp-rate Limitation of Cable-in-Conduit Conductors," <i>IEEE Transactions on Applied Superconductivity</i> : vol. 3, no. 1, 1993).	40
4.2	The results from the ramp rate limitation test in which the background field was held constant at 11 T, 12 T, or 13 T (curves marked in the figure) while the sample current was ramped at constant ramp rate. The current at which a resistive electric field as defined by the criterion was detected has been normalized to the critical current.	44

- 5.1 A plot of Eq. 5.3 showing qualitatively the predicted quench current as a function of ramp time and effective transverse resistivity using parameters from the DPC-EX coil, assuming AC losses are the only energy disturbance to the cable. The dotted line suggests an approximate relationship a computer solution to the stability problem with AC losses during ramping conditions might produce. 50

LIST OF TABLES

1.1	Major parameters of the sample coil used in the experiments in the thesis.	21
-----	---	----

CHAPTER 1

Introduction

1.1 Overview

As current world energy sources become more scarce, the search for reliable new energy sources becomes more important. One promising new form of energy conversion is fusion, which uses the same basic nuclear reaction as the sun to produce energy. The intense temperatures required for a sustained fusion reaction—tens of millions of degrees—make heating and containing the fusing material the major obstacle in realizing fusion power production.

One proposed solution to this problem consists of using magnetic fields to both contain and heat the hot plasma. In the 1950's, L. A. Artsimovich and A. D. Sakharov suggested using a toroidal magnet for plasma containment (Iwasa, 1994). This toroidal coil magnetic confinement machine, or "tokamak," could then use a poloidal coil to

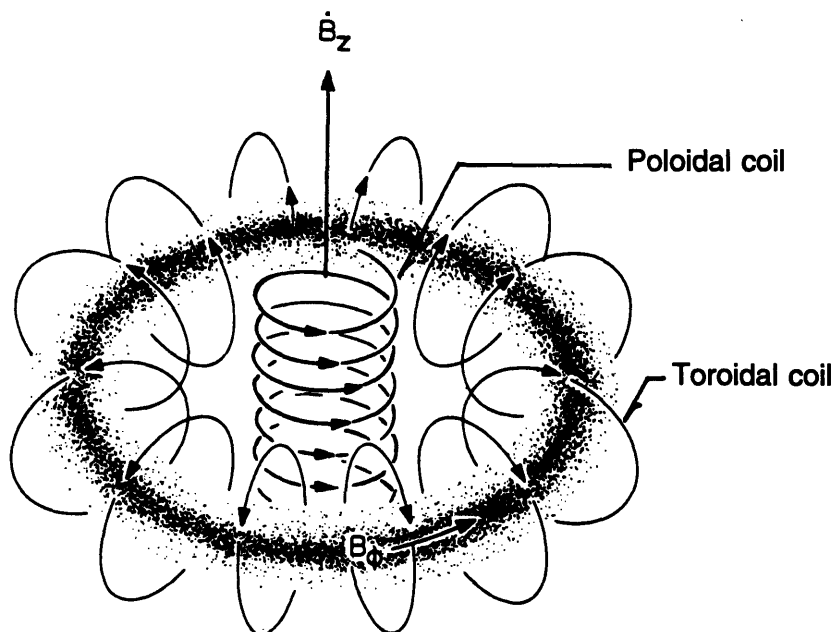


Figure 1.1 Schematic drawing showing two principal coils (and fields) in a tokamak. The toroidal field provides B_θ for plasma stability, while the poloidal coil in the center provides B_z for plasma heating. (from M. N. Wilson, *Superconducting Magnets*, Clarendon Press: Oxford, 1983)

provide a changing magnetic field that would accelerate the plasma and provide heating to the requisite temperatures. (See Fig. 1.1)

Unfortunately, conventional (resistive) magnets made from typical engineering materials would require more power to create the necessary magnetic fields and to cool the magnet windings (to prevent overheating) than the tokamak would produce. Since using conventional magnets will not yield a commercially viable reactor, research into superconducting magnets has increased. However, while superconducting magnets do not suffer from the same energy consumption requirements as their conventional counterparts, they have other problems that must be overcome before an energy-producing reactor can be built.

Most important are the requirements for maintaining superconductivity. An engineering-grade superconductor has a normal resistance on the order of a thousand times that of standard magnet conductors (like copper) under similar conditions (Orlando, 1991); hence, any benefit of using a superconductor is more than offset by the degraded, dangerous, and possibly violent consequences of a superconducting-to-normal transition. In order to be of benefit, then, the requirement is simple: the superconducting magnets must produce the required magnetic fields in the required space without a transition to the normal state.

Current projects to produce next generation tokamak fusion devices (such as the International Thermonuclear Experimental Reactor, or ITER) plan to use superconducting magnets for the toroidal and poloidal field coils. While the toroidal field would operate essentially in "DC mode," the poloidal field is to be generated by the central solenoid undergoing a linear current (and, therefore, magnetic field) ramp (Isono, 1993). Both the poloidal coil and the central solenoid will probably be made from cable-in-conduit (CIC) conductors (Ando, 1988). Fig. 1.2 shows the cross-sectional view of a typical CIC conductor containing a 48-strand cable.

Cable-in-conduit conductors were first proposed at MIT by Hoenig and Montgomery in the early 1970's as a way to increase the stability of superconductors above the then-available "adiabatic" magnets (Iwasa, 1994). A CIC conductor consists of many twisted strands, each of which contains many twisted filaments of superconductor

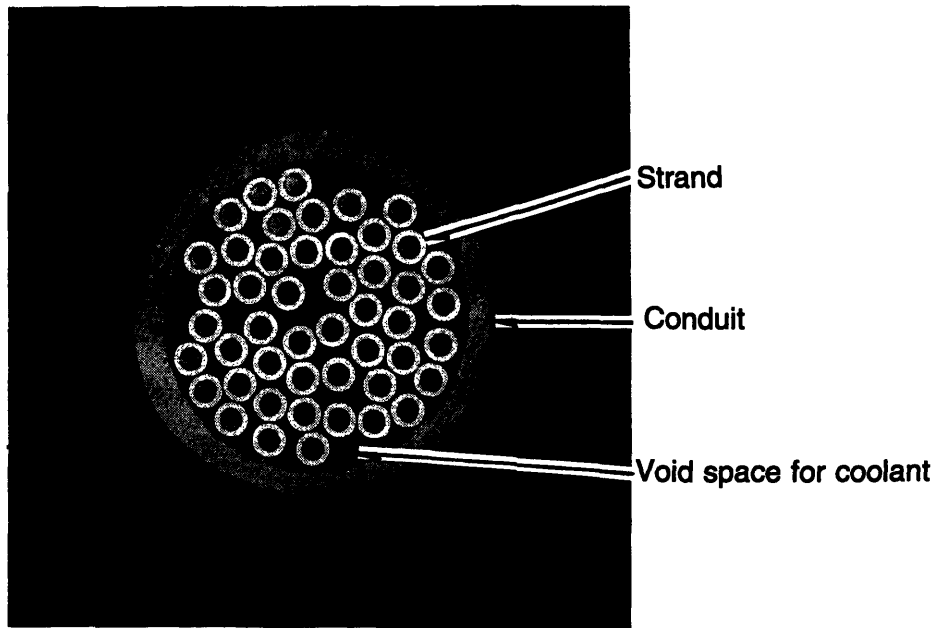


Figure 1.2 Cross section of a typical cable-in-conduit (CIC) conductor. This conductor has 48 strands: three wires twisted in triplets, then four triplets twisted in a group, and finally four groups twisted together and compacted inside the conduit. (from R. J. Nelson, "An Investigation of A.C. Losses in Two Sub-size Conductors for the ITER," JAERI-M 93-219: 1993)

co-processed with a non-superconducting metal (usually copper). The twisted strands are compressed within a conduit, providing both structural support and a passage through which liquid helium flows as a coolant. Such conductors are best suited for the large-scale, high-current applications required in a tokamak.

It has long been known that magnets made from superconducting cables, including CIC conductors, dissipate energy in the presence of changing magnetic fields; such losses are typically called "AC losses" (Wilson, 1983). These losses may jeopardize the stability of the magnet because the energy associated with these losses may cause the magnet to become "normal" instead of remain superconducting. In fact, in the context of CIC conductors for tokamaks, AC losses by means of strand-to-strand coupling have long been one of the chief concerns. However, recent discoveries have indicated that there may exist a practical limit to the reduction of these losses. Indeed, complete elimination of coupling between strands results in a CIC conductor with severely degraded performance (Turck, 1992).

This thesis investigates the stability characteristics of a typical CIC superconductor in order to determine how to optimize a magnet designed for use under the transient conditions of the central solenoid of a tokamak. The rest of this chapter is devoted to a review of basic superconducting properties in general, and of CIC conductors in specific. Specifications for the sample coil used in the experiments are also given.

Chapter two explains the AC loss experiment. This experiment determines one of the main parameters characterizing the coupling loss in a typical CIC superconductor: the coupling time constant.

The third chapter analyzes the stability experiment for the typical CIC cable under DC conditions using short heating lengths to simulate a disturbance.

Chapter four investigates the "ramp rate limitation," examining the results of the maximum current attainable under a linear ramp rate.

The final chapter discusses the connection between the three experiments, and proposes a procedure to maximize the stable current attainable in ramping magnets made with CIC conductors by determining the optimum strand insulation.

1.2 Background

This section summarizes some of the basic characteristics of superconductors. AC loss, stability, and ramp rate limitation concepts are then briefly reviewed to build a foundation for the experiments and analyses in the subsequent chapters.

1.2.1 Properties of Superconducting Materials

Superconductivity is a set of thermodynamic states in some materials in which the electrical resistivity of the substance is zero. The superconducting states are defined principally by the three interdependent quantities of critical temperature (T_c), critical current density (J_c), and critical magnetic field (H_c). Relationships between these three quantities for which a substance is superconducting define a critical surface in temperature--current density--magnetic field space. (See Fig. 1.3) The critical surface is different for each substance that allows superconducting states, and above this critical surface the substance is "normal," or resistive. Although the critical current density may

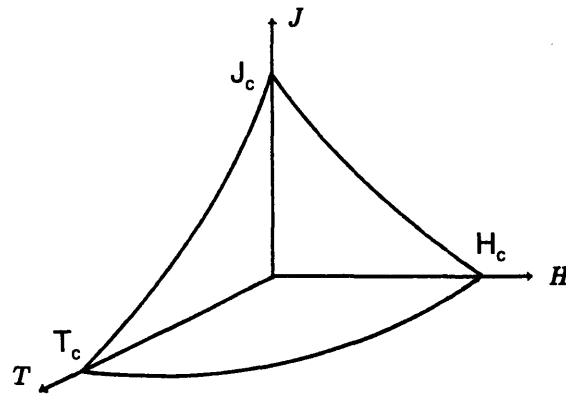


Figure 1.3 The critical surface of a typical engineering grade superconductor in temperature-current density-magnetic field space. States below the critical surface are superconducting, while states above the surface are "normal," or resistive. (from Y. Iwasa, *Case Studies in Superconducting Magnets: Design and Operational Issues*, Plenum Press: New York, 1994)

be affected by certain processing techniques, the critical surface can be thought of as a property of the specific material (Wilson, 1983).

Not all materials exhibit superconducting behavior, and among the thousands of known materials that do, very few are useful for engineering applications. In order for a substance to be of practical use, it must (among other things) be plentiful enough for the application, ductile enough for the manufacturing process, and of sufficiently high critical values to remain superconducting in the proposed operating environment. To date, the most important superconductors for engineering applications are alloys of niobium and titanium, NbTi, and an intermetallic compound of niobium and tin, Nb₃Sn (Iwasa, 1994).

Applications that rely on superconductors must always be designed so that the superconductor reliably operates below the critical surface. If a disturbance raises the state of any portion of the substance above the critical surface—for example, by an increase in temperature above the critical temperature for the magnetic field and current density present—the material undergoes a transition to the normal state, generating Joule heat. If the generated energy is not adequately removed, the Joule heating will raise the surrounding superconductor above the critical surface, and the heating effect will propagate until the entire superconductor has been driven normal. Such an event is called a "quench."

The amount of heat generated by such a transition is a function of the normal-state resistivity, which for superconductors is high: at cryogenic temperatures, the normal state resistivity of NbTi or Nb₃Sn is 100 to 1000 times greater than copper (Orlando, 1991). To reduce the Joule heating during a quench, superconducting filaments are invariably embedded in a stabilizing material that offers an alternate, low-resistance path to the current in case of quench. Usually the superconductor is co-processed with copper as the matrix material because of copper's low electrical resistivity, good thermal conductivity, and excellent mechanical properties. In the event a portion of the superconductor is driven normal, current will commutate into the copper around the "normal zone;" with adequate cooling, the Joule energy will be removed and the entire zone will return to the superconducting state. This event is called a "recovery."

1.2.2 Superconducting Strands

The superconducting materials NbTi, Nb₃Sn, and similar substances are magnetic materials, i.e. they become magnetized in the presence of a magnetic field. In the early 1960's a thermal instability known as "flux jumping" was discovered in which the energy associated with the penetration of magnetic field into a magnetic material may cause the material to quench. Further study showed that the criterion for predicting a flux jumping event depends on the physical dimensions of the superconductor, and that the smaller the superconductor, the more stability against flux jumping (Wilson, 1983). As a result, all present-day superconducting wires are manufactured by combining many tiny superconducting filaments into a composite strand with copper. For example, the strands used in the experiments described in this thesis contained 22,591 filaments of Nb₃Sn, each approximately 2 μm in diameter. (See Fig. 1.4.) The fine subdivision of the superconductor into filaments has made the instability due to flux jumping virtually insignificant when compared with other sources of instability.

In addition to flux jumping, energy can be deposited into the superconductor by interfilamentary coupling. During transient conditions, current may be induced to flow from one filament to another through resistive metal, generating Joule heat. The amount of interfilamentary coupling current depends on the induced voltages between filaments,

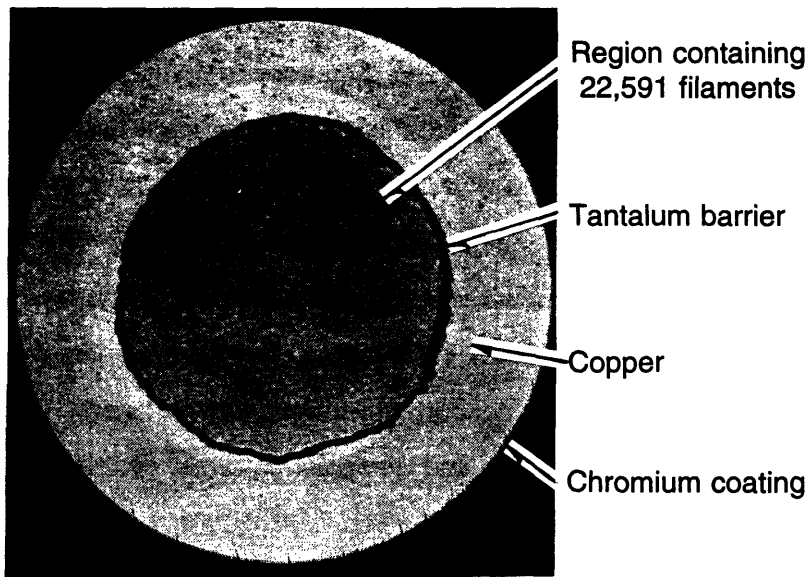


Figure 1.4 A single 0.92-mm diameter strand of a typical Nb₃Sn conductor, containing 22,591 Nb₃Sn filaments, with some niobium and bronze, surrounded by a tantalum barrier and a copper stabilizer. A layer of chromium insulation 2 μm thick coats the surface. (from R. J. Nelson, "An Investigation of A.C. Losses in Two Sub-size Conductors for the ITER," JAERI-M 93-219: 1993)

which can be made small by decreasing the area through which the changing magnetic field passes. For this reason, the filaments in a superconducting strand are twisted.

1.2.3 Cable-in-Conduit (CIC) Conductors

Cable in conduit (CIC) conductors were first developed in the early 1970's for large scale applications requiring high currents, such as fusion reactors (Iwasa, 1994). Encasing many small superconducting strands in a conduit provides two major advantages over a "monolithic" design using one large wire. First, the conduit provides structural support for the cable against the tremendous Lorentz forces it experiences while carrying a high current in the presence of a strong magnetic field. Second, this geometry provides better cooling because of the higher surface area to volume ratio.

Use of a multiple-stranded cable instead of one large wire introduces other problems, however. The strands tend to be electrically coupled in the presence of a changing magnetic field according to Faraday's law of induction, similar to the coupling

effect among filaments. Energy deposited into the conductor because of strand-to-strand coupling must be removed by the cooling. Reduction of this coupling loss to increase stability is one of the main concerns facing design engineers today.

1.2.4 AC Losses

Since CIC conductors are typically very long, large eddy current loops can be induced every time a change in magnetic flux occurs. Consequently, the strands are always transversed to minimize the area through which the magnetic field changes. The maximum induced voltages—and, hence, the induced currents—will be proportional to the twist pitch length instead of the entire length of the cable. The minimum twist pitch length is limited mainly by possible damage to the superconductor at larger and larger strains.

Although a simple twisting of the multiple strands in the CIC conductor drastically reduces the strand-to-strand coupling caused by a changing external field, the cable would still be subject to self-field effects. Thus any change in transport current flowing through the cable would produce a changing magnetic field of its own, creating undesirable coupling currents. This problem is overcome by fully transposing the strands during the twisting process. In a fully transposed cable, each strand occupies every radial position of the cable cross-section over one twist pitch length. Hence, each strand has the same inductance and the same net mutual inductance per unit length. Fig. 1.2 shows a cross-section of such a cable; this one is made by first twisting a set of three strands into a triplet, then twisting four triplets into a bundle, and finally twisting four bundles into the completed cable.

Since coupling loss is Joule heating created when induced currents flow across the resistive metal, another way to reduce the coupling loss is to provide electrical insulation on the surface of each strand. For this reason the strands are usually coated with a thin layer of resistive material. (In Fig. 1.4, although too thin to see, the copper is actually coated with a chromium layer 2 μm in thickness.) The theory of AC losses indicates that the higher the resistivity between strands, the lower the coupling (and, therefore, the smaller the amount of heat that must eventually be removed by the coolant) (Wilson,

1983). In addition, use of insulation materials such as chromium helps prevent sintering between the strands during heat treatment.

1.2.5 Stability

It is impossible to completely eliminate every source of energy input to a superconducting wire. AC losses, wire motion due to Lorentz forces, and nuclear heating in a fusion environment are some sources of energy deposition to the superconductor that may not be completely eradicated. If the magnet is to remain superconducting, the cooling condition must be capable of removing the disturbance heat (and remove it quickly enough) to return the magnet to the designed operating temperature before the magnet quenches; if a portion of the magnet is driven normal, it must recover. The heat transfer to the coolant must occur quickly enough because once a portion of the superconductor is heated to the local critical current for the local field and current density, the current in the wire is "shared" by the superconductor and the copper matrix. The temperature at which this occurs is referred to as the "current sharing temperature;" once the wire reaches this temperature, current sharing begins, causing further heating because of the Joule energy dissipated in the copper. Stability, then, refers to the largest amount of energy that can be deposited in the magnet without an ensuing magnet quench; hence, the stability of a magnet is usually given in terms of this "energy margin" or "stability margin" (Ciazynski and Turck, 1993).

In practice, the cooling available to the magnet depends on the operating current, and at least two cooling regimes are present. At low overall current density, the enthalpy of the helium coolant is available to cool portions of the magnet driven normal; this regime is named the "well-cooled" region. At high current densities, however, only the heat capacity of the surrounding metal is available to remove the heat generated when a portion of the magnet becomes normal; this regime is known as "ill-cooled." Traditionally, the operating current that marks the transition from well-cooled to ill-cooled is called the limiting current (Lue, 1994).

Theoretical determination of the energy margin involves predicting the time evolution of the superconductor temperature. Due to the multitude of variables and

complexity of the equations, stability computations are inevitably performed using computer programs (for example, see Yamaguchi, 1985). Experimentally, a heater, such as an inductive heater, simulates a thermal disturbance in the conductor winding while the magnet is at constant current, and voltage taps record any resistance created by a transition to normalcy.

1.2.6 Ramp Rate Limitation

In the 1980's some large magnets, called "demonstration poloidal coils", or DPCs, were built to demonstrate the feasibility of using CIC conductors for the central solenoid of the ITER. During the demonstration runs, it was noted that the magnets did not reach their designed operating currents when the current in them or the background field to which they were exposed was ramped at a fast rate. The collection of data from

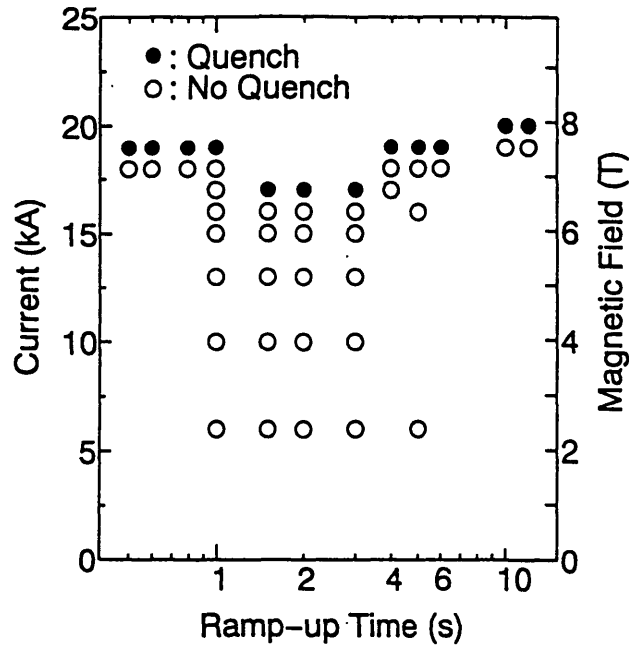


Figure 1.5 Ramp rate limitation results in the DPC-EX coil when both current and background field are ramped at a constant rate. Solid circles represent quench currents, while open circles represent stable currents. (from M. Nishi *et al.*, "Ramp-Rate Limitation Test Results of the Nb₃Sn Demo Poloidal Coil (DPC-EX)," presented at the 15th Symposium on Fusion Engineering: Hyannis, Massachusetts, October 11-15, 1993)

experiments on the DPC-EX (Fig. 1.5) and US-DPC coils both showed a degradation in highest field attainable as a function of ramp rate of either current, background field, or both (Nishi, 1993; Painter, 1992). In general, the faster the ramp rate, the lower the current at which the magnet quenched. Such a degradation could not be wholly explained by the anticipated increased AC losses as a result of a faster ramp rate, and hence became known as the "ramp rate limitation."

To date the exact cause of the ramp rate is not known, although some hypotheses include: high ramp-rate induced flux jumps, mechanical disturbances, a nonuniform current distribution among strands, abnormally high local AC losses, transverse strain degradation, and mechanical damage (Takayasu, 1993). Of these, there seems to be some evidence for non-homogeneous current distribution as a major cause (Koizumi, 1994). In fact, in many experiments in which the transverse resistance between strands is increased to extremely high values in order to minimize the AC losses, the magnets performed most poorly during a ramp (Turck, 1992). That there may be a way to optimize the stability of a ramping magnet with respect to transverse resistance is the main tenet of this thesis.

1.3 Sample conductor

Fig. 1.6 shows the sample conductor used for the experiments performed for this thesis, and Table 1.1 lists the relevant parameters. The sample is a 48-strand Nb₃Sn CIC conductor, equipped with an inductive heater, temperature sensors, and 21 voltage taps at various intervals along the conductor strands. The total length of the conductor is 6.3 m; its shape is a 10-turn solenoid. The sample was tested in the background field magnets available at the Japan Atomic Energy Research Institute in Naka-machi, Japan.

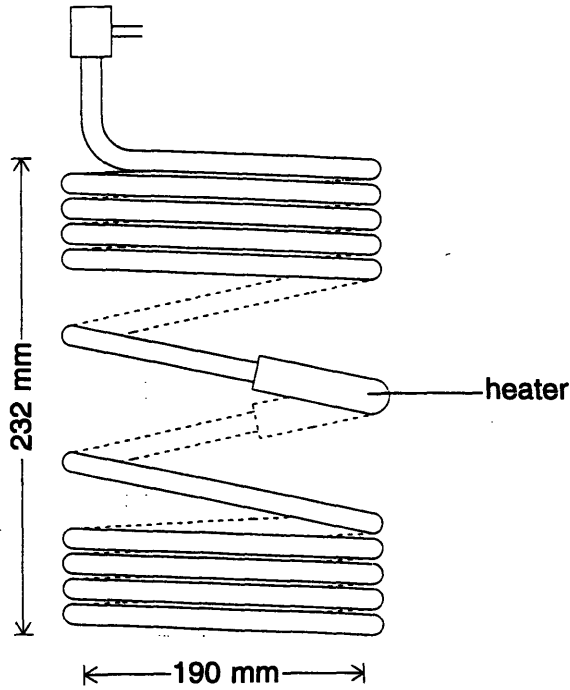


Figure 1.6 Diagram of the sample coil, used for the experiments in this thesis. The coil was wound with the CIC conductor whose cross section is pictured in Fig. 1.2. The 10-turn sample coil has a total length of 6.3 m. Other relevant parameters are noted in Table 1.1.

Table 1. Major parameters of the sample coil used in the experiments in the thesis.

<u>Strand</u>	
Superconducting material:	Nb ₃ Sn
Strand stabilizer material:	OFHC copper
Strand barrier material:	Tantalum
Strand coating material:	Chromium
Strand diameter:	0.920 mm
Filament diameter:	2 μm
Number of filaments/strand:	22,591
Filament twist pitch:	20 mm
Barrier thickness:	10 μm
Coating thickness:	2 μm
Copper to non-copper ratio:	1.58
<u>Conductor</u>	
Conduit material:	Titanium
Number of strands:	48
Void fraction (for helium):	35%
Conduit outside diameter:	9.84 mm
Conduit inside diameter:	8.06 mm
Cabling twist pitch (3 stages):	110 mm/180 mm/330 mm

CHAPTER 2

AC Loss Experiment

2.1 Overview

The purpose of this experiment was to determine the coupling time constant. As shown later, the coupling loss is proportional to this time constant; as a result, the maximum tolerable coupling time constant is sometimes stipulated in design specifications.

The experimental setup is shown in Fig. 2.1. A background field magnet subjects the sample to various magnetic environments while the pick-up coils record the sample's magnetic response. The experiment is carried out in two parts: a measurement of hysteresis loss and then a measurement of loss during transient conditions. These quantities are explained below in more detail, where the theory of AC Losses is reviewed to derive relevant expressions.

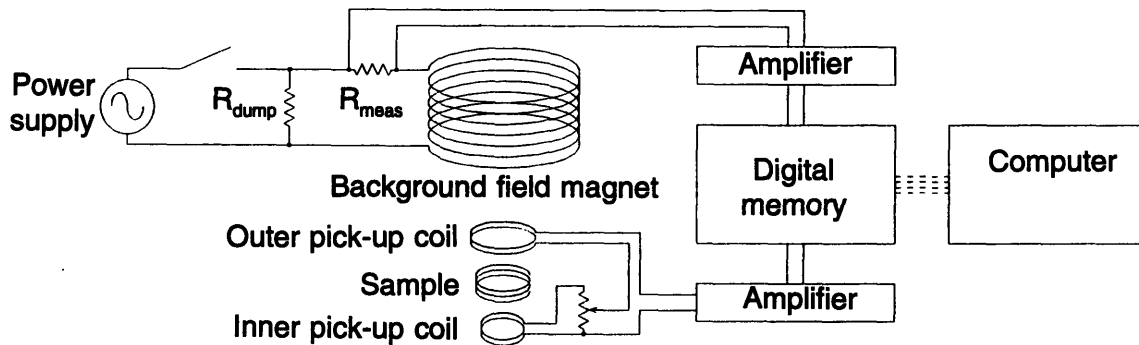


Figure 2.1 A schematic representation of the experimental setup for hysteresis loss and coupling loss measurements. From these two measurements the coupling time constant (τ_{cpl}) was determined.

2.2 Theoretical Background

The theory on AC losses has been extensively established in numerous places; hence, only an outline is given here in order to interpret the experimental results. The

Poynting power density supplied to the superconductor depends on Maxwell's equations according to:

$$-\nabla \cdot (\vec{E} \times \vec{H}) = \vec{E} \cdot \vec{J} + \frac{1}{2} \mu_0 \frac{\partial}{\partial t} (H^2) + \mu_0 \vec{H} \cdot \frac{\partial \vec{M}}{\partial t} \quad (2.1)$$

where E is electric field, H is magnetic field, J is the current density, and M is magnetization. If Eq. 2.1 is integrated over one ramping cycle (ramp up and then down), the magnetic energy storage term goes to zero, and we have:

$$Q_{loss} = \oint (\vec{E} \cdot \vec{J}) dt + \mu_0 \oint \vec{H} \cdot d\vec{M} \quad (2.2)$$

where Q_{loss} is the energy dissipated in the superconductor per unit volume. It can be shown that if the sample carries no transport current, the integrals in Eq. 2.2 can be written as (Iwasa, 1994):

$$\begin{aligned} Q_{loss} &= \mu_0 \oint (-M) dH \\ &= Q_{hys} + Q_{cpl} \end{aligned} \quad (2.3)$$

where we have written the total AC losses as the sum of "hysteresis loss" and "coupling loss." The time-independent part of the total AC losses we call hysteresis loss, while the coupling loss is the time-dependent part.

Two methods are available for measuring the AC losses from a sample carrying no transport current: calorimetry and magnetization. The former method relies on measuring the amount of boil-off of the liquid coolant as a function of time; the total losses can then be calculated by assuming the energy dissipation in the sample supplied the enthalpy of vaporization. The later method involves determining the magnetization of the sample through electromagnetic coupling. This experiment used the later.

During the experiment, the magnetization of the sample was recorded by means of two pick-up coils. The induced emf (V) around a loop of N turns, according to Faraday's law of induction, is:

$$V = \mu_0 N \frac{\partial}{\partial t} \int (\vec{H} + \vec{M}) \cdot d\vec{a} \quad (2.4)$$

The sample to be studied is placed in the bore of the background field magnet that supplies a uniform magnetic field over the sample volume. One pick-up coil (area A_i and number of turns N_i) is located inside the sample, and another (area A_o , number of turns N_o) on the outside; in this way, only the outer pick-up coil has its enclosed area pierced by the sample. The voltage signals from the two pick-up coils, each given by Eq. 2.4, are subtracted; the coils are then "balanced" (usually near $N_i A_i = N_o A_o$) so that only the magnetization portion remains, and can be determined by:

$$\mu_0 M = \left(\frac{1}{N_o A_m} \right) \int_0^t (\Delta V) dt \quad (2.5)$$

where A_m is the effective cross sectional area of magnetized material in the sample. A_m is the area the sample would occupy (inside the conduit) if the conductor were a cylindrical slab. Equating volumes of the sample with the model slab, it can be shown that:

$$A_m = \left(\frac{\pi d_i}{2} \right)^2 \left(1 + \frac{D_i}{d_o} \right) \quad (2.6)$$

where d_i and d_o are the conduit inside and outside diameters, respectively, and D_i is the inside diameter of the sample solenoid (Nelson, 1993).

One well-established theory of coupling loss in a twisted filamentary wire assumes that the composite is sufficiently fine to be treated as a homogeneous mixture (Morgan, 1970). The coupling currents will then produce a uniform internal magnetic field B_i given by the solution to:

$$B_i = B_e - \dot{B}_i \tau_{cpl} \quad (2.7)$$

where B_e is the external field, and where τ_{cpl} , the coupling time constant of the system, is given in terms of the twist pitch length l and the effective transverse resistivity ρ_{et} (including the resistance of the matrix material and the contact resistance) by:

$$\tau_{cpl} = \frac{\mu_0}{\rho_{et}} \left(\frac{l}{2\pi} \right)^2 \quad (2.8)$$

The coupling power dissipation density can be computed by integrating the Ohmic power generation for all the magnetization currents in the sample. The result is:

$$P_{cpl} = \frac{2 \dot{B}_i^2}{\mu_0} \tau_{cpl} \quad (2.9)$$

We now assume that this derivation is valid for fully-transposed cables where the individual strands take the place of the filaments in the calculation, and the twist pitch of the final cabling stage is approximately equal to the effective twist pitch. This experiment uses an exponentially decaying external field from a maximum field B_m to zero with a natural decay constant τ . Using the initial condition $B_i(0)=B_m$, we can solve for the internal field as a function of time:

$$B_i(t) = \frac{B_m}{1 - (\tau_{cpl}/\tau)} \left(e^{-t/\tau} - \frac{\tau_{cpl}}{\tau} e^{-t/\tau_{cpl}} \right) \quad (2.10)$$

The coupling loss density can then be computed in terms of the coupling time constant:

$$Q_{cpl} = \int_0^\infty P_{cpl}(t) dt = \frac{B_m^2}{2 \mu_0} \left(\frac{\tau_{cpl}}{\tau + \tau_{cpl}} \right) \quad (2.11)$$

In this experiment, the hysteresis loss (Q_{hys}) is found for the sample as the background field goes from zero to B_m and then back to zero. Then, during an exponential decay of the background field from B_m to zero, the coupling loss Q_{cpl} was calculated using Eq. 2.3. Finally, Eq. 2.11 was used to compute the coupling time constant.

2.3 Experimental Procedure and Analysis

Fig. 2.2 shows a representation of the relative locations of the sample CIC coil, the pick-up coils, and the background field magnet. The voltage across a resistor in series with the background field magnet essentially recorded the field to which the sample and pick-up coils were exposed. The pick-up coil signals were subtracted and the resulting signal integrated. No current was supplied to the sample solenoid.

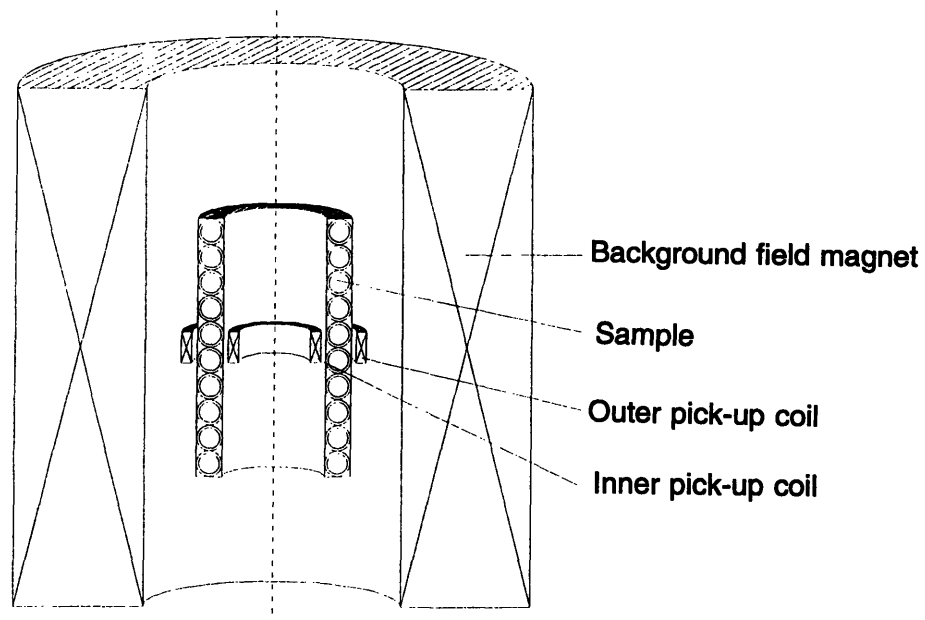


Figure 2.2 Cross-sectional cut showing the relative locations of the experimental coil and pick-up coils for the coupling loss measurement. Not to scale.

2.3.1 Determining Hysteresis Loss

After cooling the magnet and sample in a bath of liquid helium at 4.2 K, the background field magnet was energized. After a small increase in field, the field was held constant for any transient currents in the sample to decay; the background field was then increased a small amount again, and so on until the maximum field (B_m) was reached. The background field was then reduced a small amount, held steady for any coupling currents in the sample to decay, then decreased again, etc., until the field was

returned to zero. Fig. 2.3 shows the result from the hysteresis loss measurement. The area bounded by this curve represents the hysteresis loss for this particular field excitation sequence.

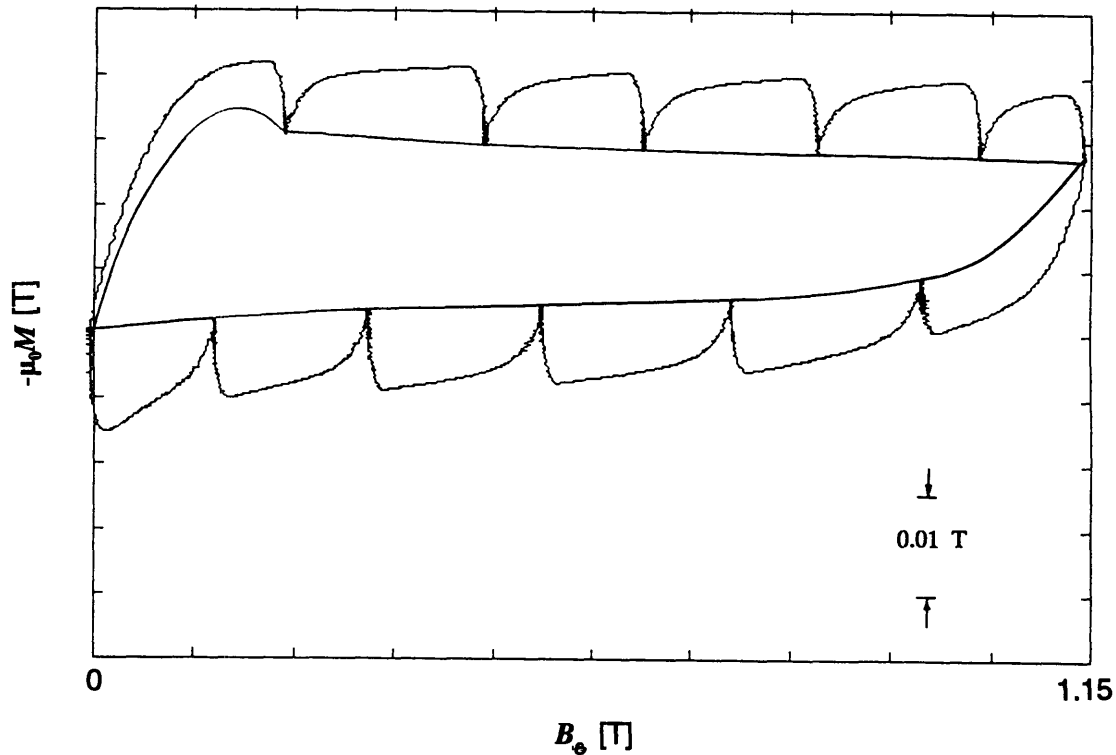


Figure 2.3 The hysteresis curve for the sample. The area inside the curve represents the hysteresis loss as the external field goes from 0 to 1.15 T and back to 0.

2.3.2 Determining Coupling Loss

After setting the background field at the highest values used during the hysteresis loss measurement and then waiting for any transients to decay, the background magnet power supply was interrupted to force the current in the background magnet (and, thus, the background magnetic field) to discharge exponentially through a resistor (R_{dump} in Fig. 2.1). The discharge resistor (R_{dump}) was changed for subsequent trials to provide different external field time constants.

For each trial the voltage signals from the pick-up coils were subtracted and numerically integrated (Eq. 2.5) with a computer program to give the energy loss data. Then the pertinent hysteretic part, previously determined from the $-\mu_0 M$ vs. B plot (Fig. 2.3), was subtracted to yield only the coupling loss. Fig. 2.4 plots the coupling loss density (energy per unit strand volume) versus the inverse of the external field decay constant τ for exponential decays of the background field from three different initial B_m .

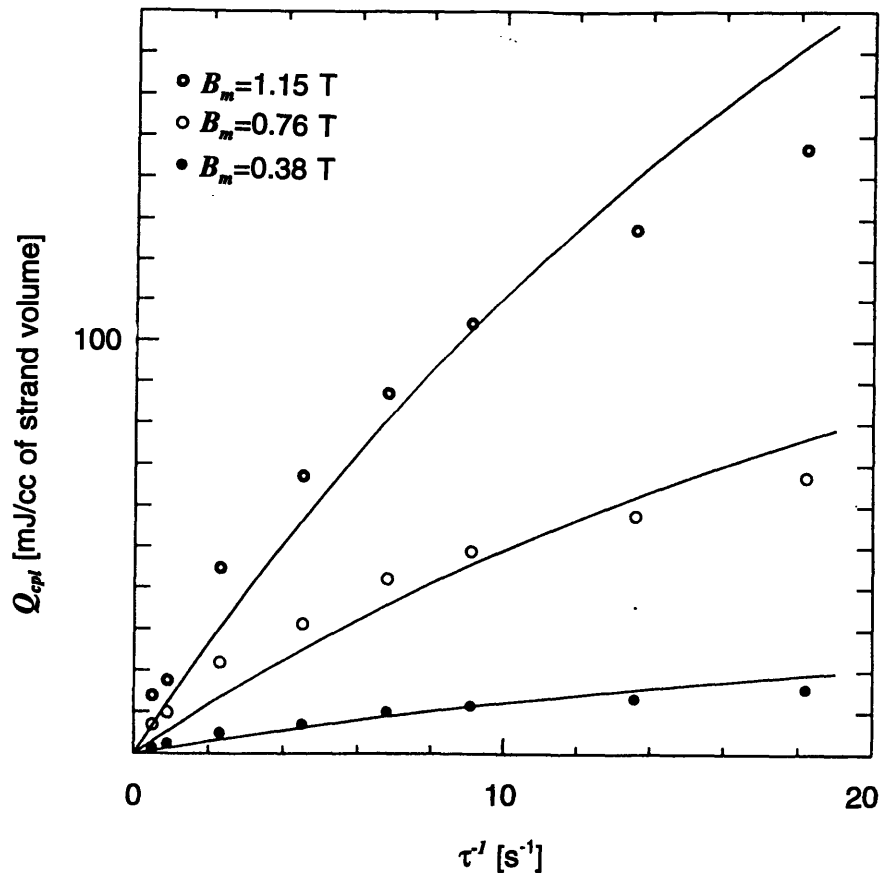


Figure 2.4 The coupling loss during an exponential dump of the background field, plotted versus the inverse of the background field decay constant. The curves, based on Eq. 2.11, show a coupling time constant (τ_{cpl}) of about 27 ms for this sample.

2.4 Results and Discussion

Using a least-squares technique, the data plotted in Fig. 2.4 were fit with Eq. 2.11 to find a coupling time constant of $27(\pm 5)$ ms. For the range of data plotted, the theory

is not exact, however: the theory was derived for simply-twisted cables modeled as a homogeneous mixture of superconductor and non-superconducting matrix, not a fully-transposed cable in which each strand is not in continuous contact with the others. Notwithstanding these assumptions, the experiment demonstrates a simple way to extract a good estimate of the coupling time constant.

Eq. 2.8 and this set of experimental data indicate that the effective transverse resistivity between strands in the conductor is $1.3 \times 10^{-7} \Omega\text{m}$. This value is at least three orders of magnitude higher than the resistivity of copper at 4.2 K, indicating that most of the resistance between strands occurs from the sum of two main parts: the resistance of the chromium insulation and the contact resistance.

In order to keep the coupling loss low, it is advantageous to have a small coupling time constant. For this sample, a coupling time constant of 27 ms is about an order of magnitude greater than that required for the central solenoid of the ITER (Nelson, 1993). However, it may be possible to control, at least in part, the coupling loss through variation of the type and amount of resistive plating on the strand surface: preliminary results from subsequent experiments show that doubling the thickness of the resistive coating reduced the coupling loss by a factor of ten. This subsequent experiment did not control for different manufacturing processes of the strands or the different void fractions, (the fraction of the cable cross section occupied by helium, which may influence the compaction of the strands inside the conduit) (Nelson, 1994). Nevertheless, such experiments suggest that control of the coupling loss by means of careful selection of coating resistivity may be possible.

To simulate a thermal disturbance, an inductive heater was placed on the central winding of the sample, where the highest magnetic field is attained. The background field magnet produced a constant field of 13 T, a typical peak field the central solenoid of the ITER is to endure (Ando, 1988). Voltage taps at several locations on the sample recorded any resistive transition.

3.2 Theoretical Background

Theoretically, a solution to the time-dependent energy equation for the superconductor, non-superconducting metal, and the liquid helium inside the conduit is sufficient to determine the energy margin of the conductor; this involves the simultaneous solution of the Navier-Stokes equations for the helium as well. Unfortunately it is not usually practical to solve all the equations in four dimensions (three spatial variables and one temporal variable) for every conceivable configuration and disturbance possibility because of the enormous computing time required. Consequently, several stability models have been developed based on simplifications of the equations, and many have been programmed as computer simulations (for example, see Yamaguchi, 1985).

Even with the difficulty in predicting exactly how much energy deposited into the winding will produce a quench, some limiting circumstances can help narrow the range of possibilities. At low operating currents, the heat capacities of the wire and the helium are available to remove the energy until the operating temperature is restored, although typically the helium enthalpy is much greater than that of the wire. In terms of the energy density,

$$\begin{aligned} \Delta E &= \int_{T_{op}}^{T_{cs}(I_{op})} \left[\left(\frac{A_{He}}{A_{me}} \right) \gamma_{He} c_P(T) + \gamma_{me} c_{me}(T) \right] dT \\ &\approx \frac{A_{He}}{A_{me}} \int_{T_{op}}^{T_{cs}(I_{op})} \gamma_{He} c_P(T) dT \end{aligned} \quad (3.1)$$

where A_{He} and A_{me} are the cross-sectional areas of the helium and the metal, respectively; T_{cs} is the current sharing temperature (see below); and γ and c represent the mass density

and specific heat of the metal ("me") or helium. CIC conductors with stability margins approaching this limit operate in what has traditionally been termed the "well-cooled" regime.

At very high currents we expect there will be little time for effective heat transfer to the helium. In this regime, only the enthalpy of the conductor can absorb the energy. Thus the lower limit is just:

$$\Delta E = \int_{T_{op}}^{T_{cs}(I_{op})} \gamma_{me} c_{me}(T) dT \quad (3.2)$$

Magnets operating with stability margins approaching this limit are said to be operating in the "ill-cooled" regime.

In both of these limits, the current sharing temperature is a decreasing function of operating current. Provided the magnetic field is constant, the dependence is usually given by a linear relationship:

$$T_{cs} = T_{op} + (T_c - T_{op}) \left(1 - \frac{I_{op}}{I_c} \right) \quad (3.3)$$

where T_{cs} , T_c , and T_{op} are the current sharing temperature, the critical temperature at the operating field, and the operating temperature, respectively. I_{op} is the operating current and I_c is the critical current at the operating temperature.

The boundary between the well-cooled and ill-cooled regimes is traditionally characterized by a current known as the limiting current (Bottura, 1994). The theoretical value of this current can be estimated by using the Stekly criterion, essentially equating the Joule heating produced when a superconducting wire operates at $T_{cs} < T < T_c$ to the cooling power supplied by the heat transfer to the helium. This value can be determined as:

$$I_{lim} = \sqrt{\frac{h f P A_{me} (T_c - T_{op})}{\rho_{me}(B)}} \quad (3.4)$$

Here, h represents the heat transfer coefficient, assumed temperature-independent, between the strands and the helium; A_{me} and P represent the cross-sectional area of the matrix metal and the perimeter of the strands; f is the fraction of the perimeter in direct contact with the helium; and ρ_{me} represents the resistivity of the normal metal, which is field-dependent, but nearly temperature-independent up to about 30 K (for copper). Although h can vary over a considerable range, a value of 1000 W/(m² K) is generally accepted for magnet design (Lue, 1994).

In practice there seems to be a transition between the well-cooled and ill-cooled regimes, instead of a clear boundary like the limiting current. The limiting current defined by the Stekly criterion has traditionally marked the highest current in which the magnet is still well-cooled; however, recent computations by Ciazynski and Turck (1993) show that it is more correct to label the limiting current as the lowest bound of the ill-cooled regime. This means that magnets designed with an operating current below the limiting current may not have the expected stability of the well-cooled regime.

Stability experiments (like the one reported in this chapter) use a heater to deposit energy into the winding. The Stekly formula with constant heat transfer coefficient h does not take into account the limiting current's possible dependence on heating length and heating time, as well as void fraction and strand diameter. A semi-empirical formula taking these and other factors into account was produced by Dresner and modified by Lue and Miller (Miller, 1985) as a correlation of the available data on stability tests for CIC conductors:

$$h = \frac{k^2}{D_{hf}} \left(\frac{l^2}{t_H} \right)^{2/15} \quad (3.5)$$

where k is a function of helium pressure and temperature, t_H is the time in which length l_H of conductor is exposed to a heating disturbance, and D_{hf} is the hydraulic diameter of the helium cross section determined from the total wetted perimeter (including wetted conduit). Substituting Eq. 3.5 into Eq. 3.4 gives a modified expression for limiting current:

$$I_{\text{lim}} = k \sqrt{\frac{f_{me} A_{st} (A_{con} - A_{st}) (T_c - T_{op}) l_h^{4/15}}{\rho_{me} D_{hf} D_{hc} t_H^{2/15}}} \quad (3.6)$$

where f_{me} is the volume fraction of metal matrix material in the strands, A_{st} is the cross-sectional area of the strands, A_{con} is the cross-sectional area inside the conduit (conductor and helium), and D_{hc} is the hydraulic diameter of the helium cross section determined from only the cooled perimeter of the strands.

The resistivity of the copper stabilizer is a function of magnetic field, and above about 30 K also a function of temperature. Usually an intrinsic value (at zero field and about 20 K) is expressed in terms of the ratio of copper resistance at 273 K to its resistance at 20 K, called the residual resistivity ratio, or RRR. The superconducting magnet design criteria used for the ITER express the field-dependent copper resistivity at 4.5 K according to:

$$\rho(B) = \rho_c (1 + 0.3046 B - 6.13 \times 10^{-4} B^2) \quad (3.7)$$

where

$$\rho_c = (0.155 \times 10^{-7} \Omega \text{m}) / (\text{RRR} - 1)$$

and B is given in tesla (T) (Magnet Design Criteria, 1994).

3.3 Experimental Procedure

With the background field magnet set to 13 T, the 6-atm supercritical helium forced through the conduit at a rate of 1 g/s, and the current in the sample set, a 1-kHz pulse was sent to the inductive heater for 5 ms. The length of the heated zone was 50 mm for the first set of data, and 200 mm for the second set. If the sample did not quench, the amplitude of the heater signal was increased, and again sent to the inductive heater. This procedure was continued until the sample quenched. The sample current was then modified, the sample cooled to operating temperature, and the entire process was repeated.

3.4 Analysis and Results

The results of the measurements for two different lengths of heated regions are shown in Figs. 3.2 and 3.3, each of which shows heating energy density (over strand volume) vs. transport data. The so-called limiting current is apparent at about 1.5 kA when the heating length is 50 mm (Fig. 3.2), and at about 1.25 kA when the heating length is 200 mm (Fig. 3.3).

Without direct measurement of the residual resistivity ratio, it was still possible to estimate the resistivity of the copper stabilizer at the background field value of 13 T from the voltage rise data during a quench. Voltage taps on the sample recorded the voltage difference between different locations along the conductor. While the sample was superconducting, no voltage difference between taps was detected; when the sample quenched, the voltage difference between taps rose in the presence of the resistive electric field. For example, in Fig. 3.4, the transition from superconducting to normal can be seen for a section of the strand 317 cm long (labeled curve V5-V7 in Fig. 3.4), and between an adjacent section 162 cm long (labeled curve V7-V9 in Fig. 3.4). The quick, linear increase from zero voltage to some non-zero value is attributed to the transition, while any subsequent rise is due to a rise in the temperature as Joule heating is dissipated. Since the transition occurs quickly (during a few hundred milliseconds), we can assume the temperature is nearly constant; then the resistivity is just:

$$\rho_{me} \approx \frac{A_{me} (\Delta V)}{I_{op} (\Delta l)} \quad (3.8)$$

where ΔV is the voltage rise between taps, Δl is the length between taps, A_{me} is the copper cross-sectional area, and I_{op} is the current in the sample. Calculations for all the recorded voltage taps for all quenches indicated that the resistivity of the copper stabilizer at 4.5 K and 13 T was between $5.5 \times 10^{-10} \Omega\text{m}$ (RRR value of 138 by Eq. 3.7) and $7.5 \times 10^{-10} \Omega\text{m}$ (RRR value of 101 by Eq. 3.7).

With this value of resistivity, Stekly's equation (Eq. 3.4) predicts a limiting current of about 4.2 kA, with a nominal heat transfer coefficient of $1000 \text{ W}/(\text{m}^2 \text{ K})$ and an estimated 60% fraction of strand perimeter wetted by the helium. The empirical

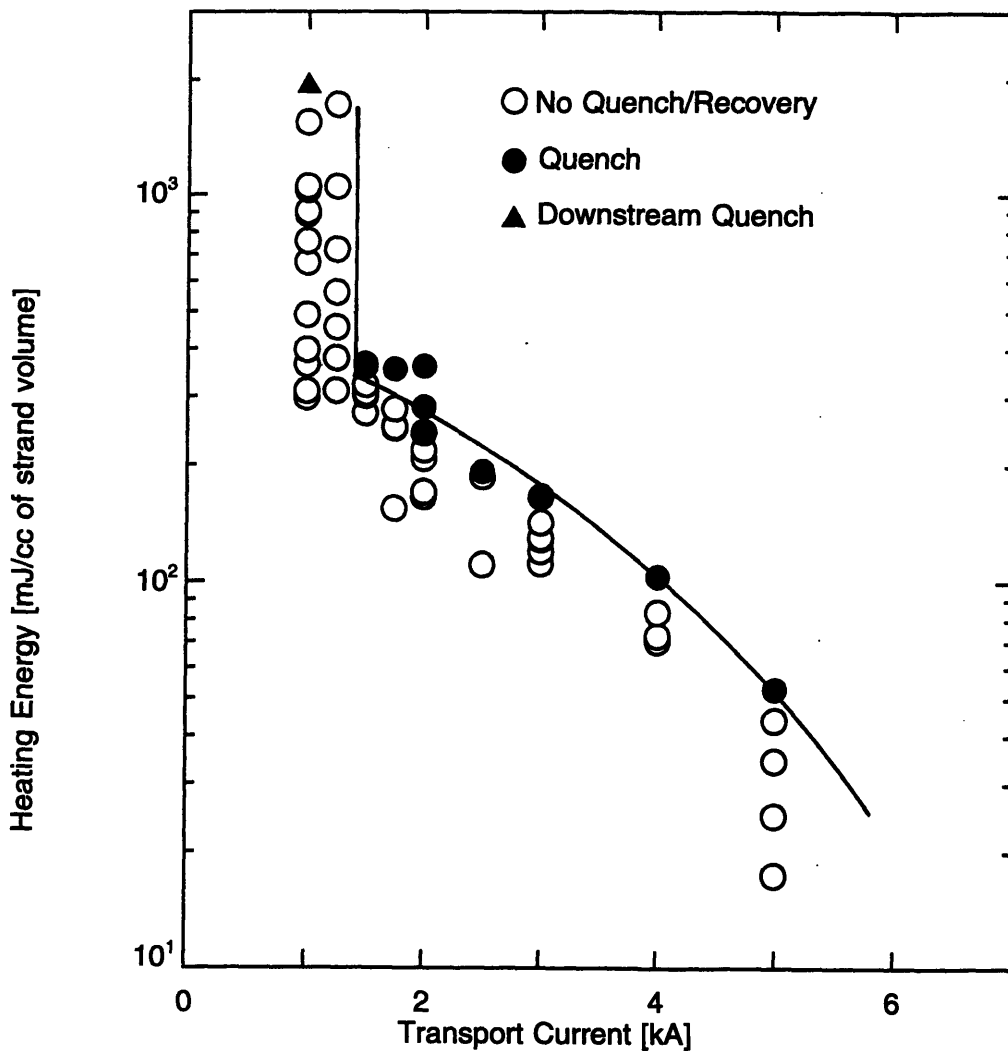
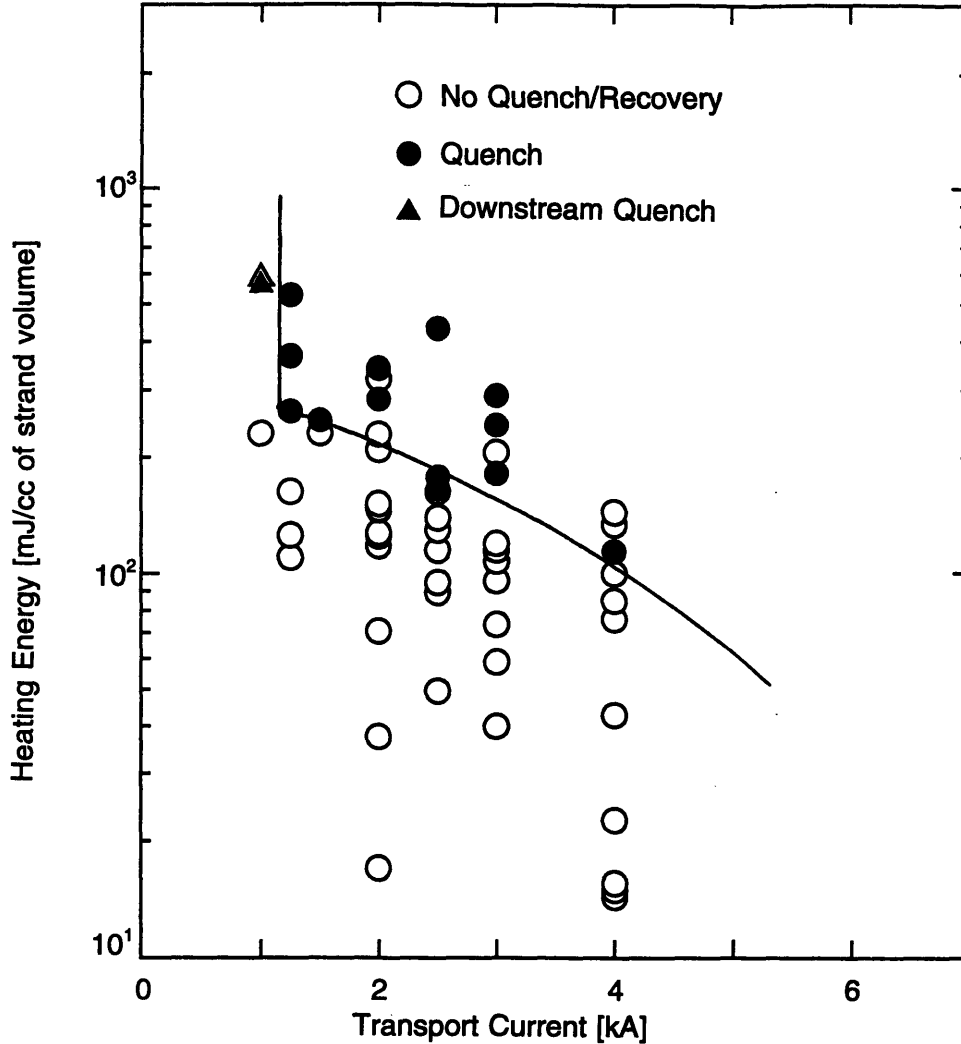


Figure 3.2 The stability margin plotted versus operating current for an inductive heating length of 50 mm. Open circles represent stability after energy deposition; solid circles represent magnet quench. The solid triangle indicates a quench initiated far downstream from the heated region.

correlation given by Eq. 3.6 is slightly more realistic, yielding a limiting current of 2.5 kA for a 50-mm heating length, and 3.0 kA for a 200-mm heating length.

Below the limiting current, the maximum output from the inductive heater could not force the magnet to quench, except in a few instances where the energy removed by



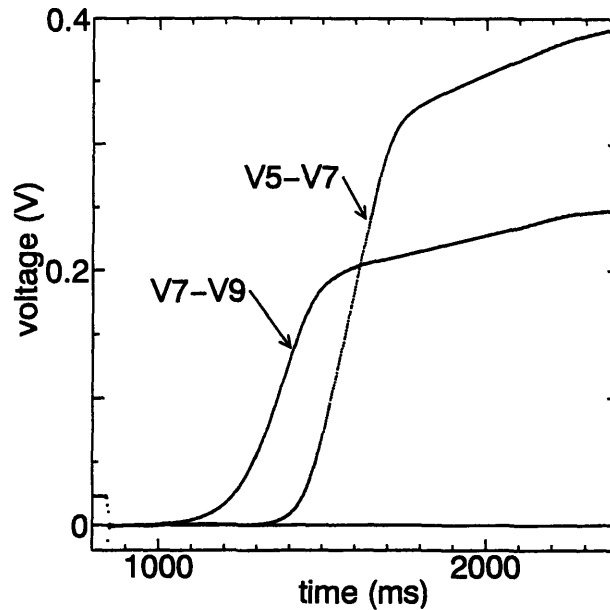


Figure 3.4 A typical recording of the voltage rise caused by superconducting-to-normal transition during a quench. The trace marked V5-V7 corresponds to the voltage difference between voltage taps placed 317 cm apart; the trace marked V7-V9 recorded the voltage difference between voltage taps placed 162 cm apart.

3.5 Discussion

The value of the copper resistivity is low compared with other typical Nb₃Sn conductors. A value of $6.5 \times 10^{-10} \Omega\text{m}$ for the copper resistivity at 4.5 K and 13 T corresponds to a residual resistance ratio of 117 (see Eq. 3.7), which is higher than the reference value of 100 used for design of the ITER, but is within the normal range $20 < \text{RRR} < 300$. Such a value is well within specifications for the ITER. Lower values of resistivity also correspond to higher values of thermal conductivity according to the Weidmann-Franz law (Wilson, 1983), a fact that may slightly increase the stability margin.

The difference between the theoretical prediction for the limiting current and the experimental value is troublesome, and the constant value of $1000 \text{ W}/(\text{m}^2 \text{ K})$ for the heat transfer coefficient must be called into question. In addition, as the heated region

increased, the limiting current decreased, in contradiction with other experiments (Armstrong, 1992) and the correlation expressed in Eq. 3.6.

It is important to note that when this stability margin experiment measures a quench, the transport current was probably distributed equally among the strands. During the procedure, after the current was set, a small energy disturbance that did not cause a quench was deposited repeatedly into the strands (open circles in Figs. 3.2 and 3.3). Koizumi (1994) reported that small energy disturbances into the strands of CIC magnets was usually enough to allow unbalanced transport currents to redistribute more evenly, thereby increasing the magnet's stability. Therefore, the stability margin was most likely recorded in this experiment without any current maldistribution.

CHAPTER 4

Ramp Rate Limitation Experiment

4.1 Overview

The purpose of this experiment was to determine the quench current dependence on the rate of ramping current. The investigation used the same experimental setup as the stability measurement (see Fig. 3.1).

4.2 Theoretical Background

As remarked in Chapter 1, the cause of the ramp rate limitation is not known. One model proposed by Takayasu (1993) seeks to predict the current at which a ramped magnet will quench without knowing *a priori* the mechanism responsible. In this model, the strands in the magnet are conjectured to be exposed to periodic energy disturbances (labeled $g(t)$ in Fig. 4.1) of duration t_d . Each disturbance is postulated to cause the

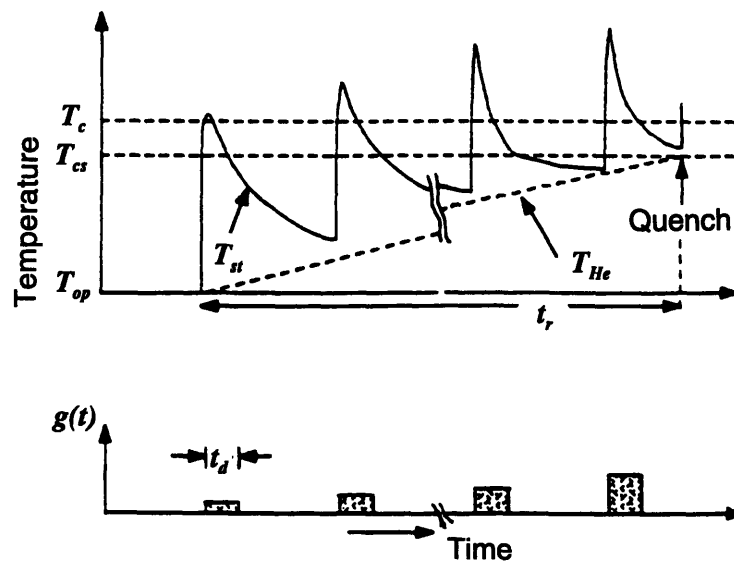


Figure 4.1 Schematic representation of the ramp rate limitation model proposed by Takayasu (from M. Takayasu *et al.*, "Measurements of Ramp-rate Limitation of Cable-in-Conduit Conductors," *IEEE Transactions on Applied Superconductivity*: vol. 3, no. 1, 1993)

temperature of a strand (T_{st}) to rise to the critical temperature, generating heat as the current is forced to flow through the copper matrix. The helium temperature (T_{He}), originally at T_{op} , increases in time as it absorbs the Joule heat and cools the strand. When the helium, assumed static, can no longer cool the strand to below the current sharing temperature before the next energy disturbance, the strand is assumed to quench. The length of time from the onset of the energy disturbances is labeled t_r .

The frequency of the proposed energy disturbances for the whole conductor is made proportional to the time derivative of the square of the magnetic induction because this proposal fit the data best. With this and other simplifying assumptions, Takayasu predicts the CIC magnet will quench under fast ramps according to:

$$I_q = \sqrt{I_{lim}^2 + \frac{\beta N^{(3-\alpha)} A_{me} \chi}{\rho_{Cu} B \dot{B}}} \quad (4.1)$$

where I_q is the predicted quench current, I_{lim} is the so-called limiting current given by the Stekly formula (Eq. 3.4), N is the number of strands in the cable, A_{me} is the cross-sectional area of non-superconducting metal, ρ_{Cu} is the field-dependent electrical resistivity of the copper, α and β are constant parameters adjusted to make the proposed model fit the available experimental data; and where χ is a cooling parameter given by

$$\chi = \frac{A_{st}}{N t_r t_d} \int_{T_{op}}^{T_{cs}} \gamma_{me} c_{me}(T) dT + \frac{Ph}{N t_r t_d} \sum_{i=0}^{(f, t_d)} \left\{ \int_{(it_p + t_d)}^{[(i+1)t_p]} [T_{st}(t) - T_{He}(t)] dt \right\} \quad (4.2)$$

In Eq. 4.2, A_{st} represents the cross-sectional area of the strands, t_r the time from the beginning of the ramp to the onset of a quench, t_d the time duration of each of the hypothesized energy disturbances, f_r the proposed ramp rate-dependent disturbance frequency, T_{st} the temperature of the strands, T_{He} the helium temperature, and all other parameters as previously defined.

Eq. 4.2 can be simplified somewhat by replacing the integrands with appropriate averages; then the parameter t_d can be incorporated into the fitting parameter β in Eq. 4.1. Finally the experimental data can be fit with Eq. 4.1 by adjusting α and β .

It is important to note that according to Eq. 4.1, any ramp rate limitation causing the magnet to quench does so at currents higher than the limiting current. This is because the limiting current (Eq. 3.4) is derived assuming the Joule heat dissipated in the conductor exactly balances the heat removed by the helium in steady state at that current, while the Takayasu model assumes the conductor dissipates Joule heat only during a fraction of the ramping time. In fact, Iwasa (1994) notes that Eq. 4.1 cannot predict a quench under slower ramp rates because the heat transfer to the helium is limited by the maximum nucleate heat transfer flux under transient conditions.

As noted, the Takayasu model does not account for the mechanism responsible for the ramp rate limitation, although there is some speculation that a maldistribution of current among the strands may play some role. Recent experiments have shown that some of the superconducting strands in a cable may carry a larger share of the transport current than others (Koizumi, 1994); it is plausible that if the strand that carries more than the average current reaches its critical current, any excess current will be transferred to neighboring strands. If the current is not adequately transferred, the Joule heating in the strand may propagate and cause the entire magnet to quench.

Such a maldistribution of current may very well lead to a ramp rate limitation, although the cause of the maldistribution has not been precisely determined either. An investigation by Ferri (1994) modeled a 27-strand CIC conductor made of Nb_3Sn as an electric circuit of inductors (to represent the superconductor in the strands) and resistors (to represent the current paths between strands and the resistive connections between strands and the power supply current leads), and used a computer to solve for current distributions. The analysis showed great current imbalances can occur not only from strand to strand, but also at different locations along a strand during transient conditions; hence, current may be forced to diffuse across the transverse resistivity at currents even below the critical current. The degree of current maldistribution depends on the cable length, the twist pitch of each cabling stage, the transverse resistance between strands (assumed constant in the study), the resistances at the joints at either end of the cable, and the ramping rate (of background field, self field, or both). Because of the profuse number of simultaneous equations to be solved, any specific solution must be found by computer.

Based on the computer simulations, Ferri proposes that the ramp rate limitation may be due to the low transverse resistance between strands in the joints where the cable is soldered to the connecting circuitry. This model assumes the transverse resistance in the joints is much smaller than in the cables, although precise measurements do not currently exist. However, the model does indicate that there exists a finite quench current as the ramp time tends to zero, although different from the limiting current present in Takayasu's proposal.

4.3 Experimental Procedure

With the background field set to 13 T, and the forced-flow coolant constant at a pressure of 6 atm and flow rate 1 g/s, the current in the sample was ramped from zero current at a fixed ramp rate until a resistive electric field greater than 0.1 $\mu\text{V}/\text{cm}$ was detected. This resistive electric field criterion was used throughout to indicate the sample was no longer superconducting. The current was returned to zero and then ramped at another rate; the current ramp rates ranged from 0.5 kA/min to 50 kA/min. The process was repeated for background fields of 12 T and 11 T.

4.4 Analysis and Discussion

The results from the ramp rate test are shown in Fig. 4.2, where the resistive current normalized to the critical current is plotted against the ramp rate. The normal current, when the sample would presumably quench without recovery, shows a very weak dependence on the current ramp rate.

A computer program was used to calculate the maximum *field* ramp rate to which the winding was exposed—i.e., the maximum self-field ramp rate—which occurs at the maximum current ramp rate of 50 kA/min. The analysis showed a maximum field ramp rate in the coil of 0.05 T/s—a very small value compared with the anticipated 13 T/s ramp expected in the central solenoid of the ITER and experienced by the DPC-EX. Thus, while the current ramp rate is high, the resulting field ramp rate is low, and we conclude that the instability caused by the ramp rate phenomenon is most likely triggered by a ramping magnetic field within the winding.

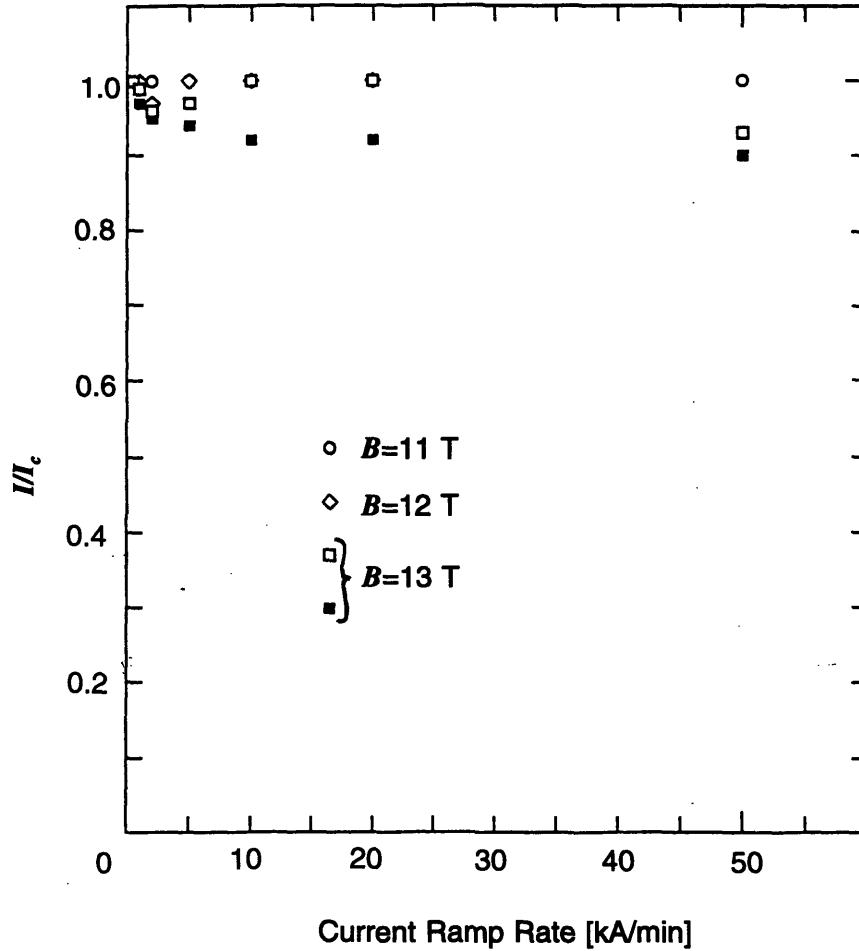


Figure 4.2 The results from the ramp rate limitation test in which the background field was held constant at 11 T, 12 T, or 13 T (curves marked in the figure) while the sample current was ramped at constant ramp rate. The current at which a resistive electric field as defined by the criterion was detected has been normalized to the critical current.

The ramp rate test could not be performed with a changing background field for lack of a pulse magnet. Some results of ramp rate limitation tests in changing fields is found in the literature.

CHAPTER 5

General Discussion and Recommendations

5.1 Maximizing Magnet Stability Using Transverse Resistance

This thesis has presented some experimental results from research that define the stability of a magnet intended for use under transient conditions in general and in the central solenoid of the ITER in specific. Traditionally, the stability of a magnet answers the question, "What energy density can be deposited in the magnet by disturbances without a subsequent magnet quench?" It is obvious from the recent discovery of a legitimate ramp rate limitation, however, that traditional stability margin calculations are inadequate, at least when large magnetic field changes are present.

In general, the stability criterion for the magnet should include the ramp rate limitation. For ramping current and/or field, the stability margin should also answer, "For a given magnet and ramp rate, what is the largest current to which the magnet may be ramped without a subsequent magnet quench?" The answer to this question is more difficult than the former because it is extremely difficult, if not impossible, to know the causes and magnitudes of all the disturbances beforehand. However, as a design issue, two sources of disturbances are now familiar: AC losses and the source of the ramp rate limitation.

The AC loss experiment demonstrated that the simple filamentary theory adequately explains the expected loss. These AC losses will be distributed more or less uniformly throughout the cable cross section, but will vary from place to place due to differences in the magnetic field. Obviously the smaller the AC losses the more stable the magnet will be. Chief among these losses is the coupling loss, especially for ramping magnets, because the coupling loss depends on the changing magnetic field. Limiting the coupling loss means minimizing the coupling time constant (Eq. 2.11), and after selecting the optimum twist pitch, the effective transverse resistivity is the last parameter the magnet designer can alter; indeed, the results from the AC loss experiment suggest that at least some control over the selection of transverse resistance is available.

Which transverse resistance to choose to minimize the AC losses is simple: the larger the transverse resistance—including resistive oxide layers and the contact resistance between the strands—the smaller the AC losses and thus the larger the stability margin during ramp. But experience has shown that when the resistance is too high, the degradation due to the ramp rate limitation is severe. It has been hypothesized that the reason for the ramp rate limitation is a maldistribution of transport current among the strands, caused perhaps by unequal joint resistances and disparity among the self and mutual inductances from strand to strand. Thus the ability for current to commute away from the strands that first begin to carry the critical current to other strands that carry less is the determining factor in the instability that causes the ramp rate limitation. This commutation depends on the transverse resistance; hence, it is probable that the larger the transverse resistance, the more severe will be the limitation.

The question of which transverse resistance to choose thus becomes more difficult with the existence of the ramp rate limitation. However, it may be possible to maximize the quench current as a function of transverse resistance for a given magnet and ramp rate because the stability experiment is actually a way to examine the effect of known disturbances *except* the disturbance responsible for the ramp rate limitation. Such a determination might proceed as follows:

- (1) Determine the AC losses for the magnet as a function of ramp time and effective transverse resistivity—our first experiment;
- (2) Determine the stability margin as a function of operating current for the distributed disturbance caused by the anticipated AC losses—our second experiment;
- (3) Equate the AC losses with the stability margin and solve for quench current as a function of transverse resistivity and ramp time;
- (4) Analytically determine the quench current as a function of transverse resistance and ramp time for disturbances caused by non-homogeneous current distribution among the strands;

- (5) Design the magnet to have the transverse resistance corresponding to the highest predicted quench current for the proposed operating ramp rate of the magnet.

Details of the above plan are found in the following sub-sections.

5.1.1 Determination of Anticipated AC losses

The estimated AC losses in the magnet can be computed using the prevailing theory, as summarized in Chapter 2. The AC losses can be considered a distributed energy disturbance during the ramp that reduces the magnet stability margin.

The energy density must necessarily vary at different locations along the length of the conductor due to differences in magnetic field, and hence depends on geometry. For example, for the DPC-EX coil, which was shaped as a double pancake, the anticipated AC losses along the conductor under a linear ramp from $I=0$ to $I=I_m$ in the presence of no external field vary from the inside location at $z=0$ to $z=L$, where L represents the length of the cooling path. For ramp rates near the design value of 40 kA/s, the coupling loss dominates the AC losses, and varies according to:

$$\dot{Q}_{AC\ loss}(z) \approx \frac{k_1}{\rho_{ef}} \left(\frac{I_m}{t_r} \right)^2 \left(1 - \frac{z}{L} \right)^2 \quad (5.1)$$

where k_1 represents a constant that does not depend on time or location. Eq. 5.1 is simplistic in that it assumes the magnetic field due to transport current in the magnet varies linearly from zero outside the magnet to its maximum value at the innermost turn, and that the magnetic field is everywhere parallel to the poloidal axis of the magnet. Nevertheless, Eq. 5.1 demonstrates that the energy deposited in the winding of the magnet is distributed along the conductor path. Any computer quench analysis that solves the energy and Navier-Stokes equations in order to determine the thermal response to the AC losses must consider an equation such as Eq. 5.1 as the driving function. For geometries

different than the DPC-EX, the spacial dependence of AC losses are not necessarily the same as Eq. 5.1, but are nonetheless easily determined.

5.1.2 Stability Against AC Losses

The prevailing stability theory is reviewed in Chapter 3. It should be noted that the many computer simulations of a magnet's response to a thermal disturbance currently available assume a uniform current distribution among the strands. The programs then solve the time-dependent energy equations for the strands and the coolant, and the Navier-Stokes equations for the coolant to determine if a thermal disturbance of specified energy and power will ultimately lead to a quench. Most of the programs currently assume a disturbance time of a few tenths of a second.

It is now proposed that the stability margin predicted by the computer simulation or by direct experimentation is valid for magnets under transient conditions as well. While an "acceptably low" AC losses value has not been defined, the energy dissipated in the magnet must at least not be larger than the stability margin for the maximum current or maximum field obtained by the magnet; that is, for stability against quench during a ramp, we must have

$$Q_{AC\ loss}(B_m, t_d, \rho_{ef}) \leq \Delta E(B_o, I_{op}) \quad (5.2)$$

where B_o is the background field, and I_{op} the steady current used in the stability calculation. Equality in Eq. 5.2 signifies the magnet will quench at $I_q=I_{op}$ if AC losses alone are responsible for the energy disturbance. In actual magnets, the AC loss energy leading to quench may be lower than predicted by Eq. 5.2 if other disturbances—wire movement, local heat loads—are present. Current computer programs could compute the predicted quench current due to AC losses alone for most magnet geometries to determine the functional dependence on ramp time and transverse resistivity.

A rough estimate can be obtained for the predicted quench current if the stability margin is assumed to be approximately equal to the available cooling enthalpy of the helium in the well-cooled region and the heat capacity of the metal in the ill-cooled region. For example, if the field to which the magnet is exposed consists only of self

field, and if the AC losses are assumed to be deposited in the highest field region only (on the innermost turn, say), then Eq. 5.1 can be integrated and set equal to the energy margin (Eqs. 3.1 and 3.2) when the highest current equals the predicted quench current, I_q :

$$k_1 \frac{I_q^2}{t_d \rho_{ef}} \approx \begin{cases} \frac{A_{He}}{A_{me}} \int_{T_{op}}^{T_{cs}(I_q)} \gamma_{He} c_p(T) dT & (I_{lim} > I_q) \\ \int_{T_{op}}^{T_{cs}(I_q)} \gamma_{me} c_{me}(T) dT & (I_{lim} \leq I_q < I_c) \end{cases} \quad (5.3)$$

where the limiting current, I_{lim} is given by Eq. 3.4. The ramp time t_r here represents the time during which the current in the magnet increases linearly from zero to I_q .

Although Eq. 5.3 has oversimplified predicting the quench current because of the assumptions made to derive it, and a one-dimensional computer model would be more accurate, some general features of the stability of the magnet can be observed. Approximating the integrands in Eq. 5.3 as constant, Eq. 5.3 is plotted in Fig. 5.1 with parameters of the DPC-EX. The two solid lines in Fig. 5.1 represent the two regimes in Eq. 5.3 ($I_{lim} > I_q$ and $I_{lim} \leq I_q < I_c$); the dotted line shows what the actual curve might look like when Eq. 5.2 is solved by computer. Note that the larger the transverse resistivity for a given ramp time, the larger the predicted quench current. Note also that the magnet is limited by the critical current at higher transverse resistivities (and longer ramp times), as expected. For a given transverse resistivity and ramp time, the actual magnet must be ramped only to operating currents less than the predicted quench current.

5.1.3 Stability with Ramp Rate Limitation Phenomenon

Normal AC loss theory cannot explain the ramp rate limitation. Because traditional stability theories, which assume homogeneous current densities and magnetic fields among the strands, fail to predict the degraded quench current at higher ramp rates, Ferri (1994) proposes the ramp rate limitation be considered a current density disturbance assumed to take place at constant temperature. However, whether the mechanism

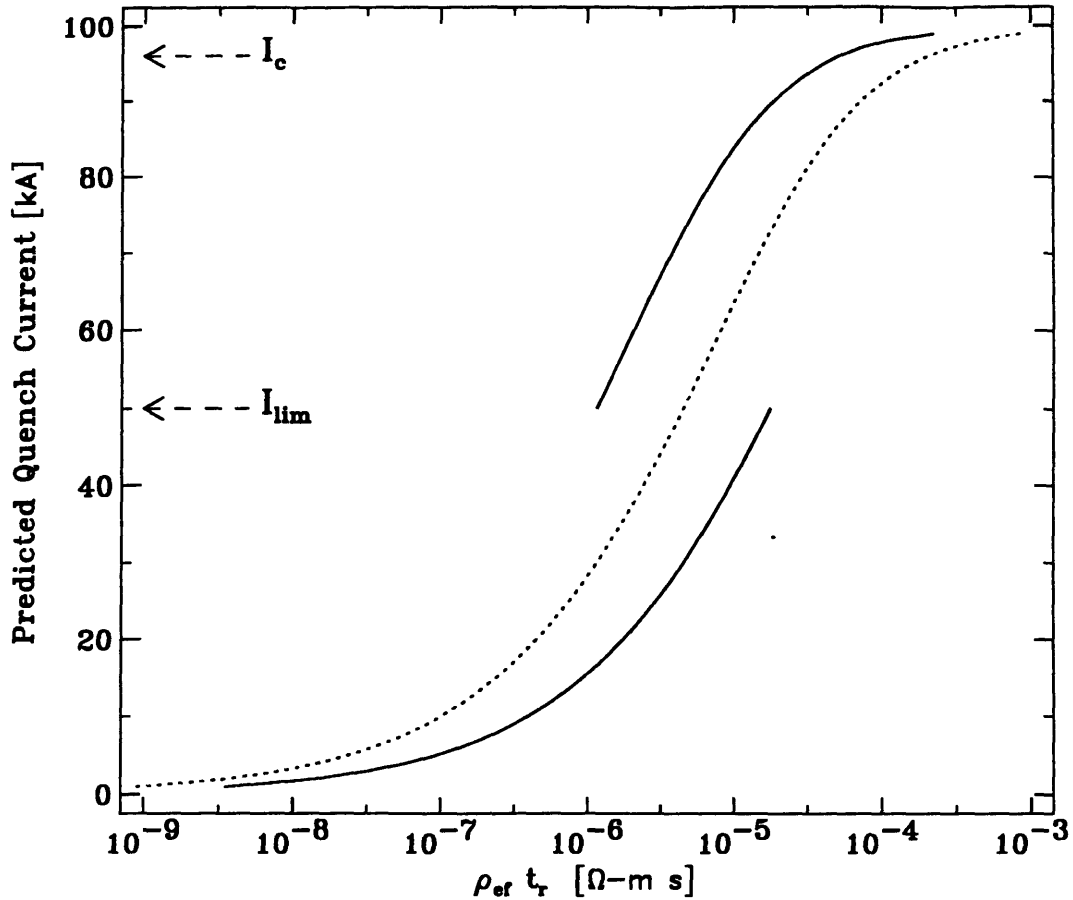


Figure 5.1 A plot of Eq. 5.3 showing qualitatively the predicted quench current as a function of ramp time and effective transverse resistivity using parameters from the DPC-EX coil, assuming AC losses are the only energy disturbance to the cable. The dotted line suggests an approximate relationship a computer solution to the stability problem with AC losses during ramping conditions might produce.

responsible for the ramp rate limitation is due to a current density perturbation or temperature perturbation, the resulting energy must eventually be removed by the coolant or else lead to a magnet quench. As a result, the ramp rate limitation may be thought of as an additional energy load on the cooling condition: an "equivalent ramp rate limitation loss."

The equivalent ramp rate limitation loss must depend on the ramp rate of the magnetic field, and thereby be partly responsible for the degraded performance at higher ramp rates. However, it is not clear whether such an equivalent energy loss necessarily

depend on the total time of ramping. Indeed, an experiment cited in Ferri (1994) showed that a 27-strand sample magnet quenched at the same current under identical ramping conditions regardless of any initial bias field, and hence suggested that this equivalent ramp rate limitation loss was not an "integrated loss." (It is not clear whether the sample had an initial current maldistribution.)

In any case, the notion of equivalent ramp rate limitation loss may be helpful in studying the phenomenon to determine the effect of transverse resistance on the maximum attainable stable current. This is because the equivalent loss idea and Ferri's current density perturbation theory both suggest that the AC losses and the ramp rate limitation effects are essentially uncoupled phenomenon. Therefore, for conductors that undergo a linear magnetic field ramp from zero to a maximum field B_m in time t_d , we can write:

$$Q_{tot} = Q_{hys}(B_m) + Q_{cpt}(B_m, t_d, \rho_{ef}) + Q_{errl}(B_m, t_d, \rho_{ef}) + Q_{other} \quad (5.4)$$

where Q_{errl} represents the effective ramp rate limitation loss, and Q_{other} represents other disturbances (*e.g.* wire motion) which may be present.

In Eq. 5.4 it is assumed that Q_{errl} depends on the effective transverse resistivity between the strands: it is hypothesized that the current redistribution around the segment of a strand driven normal by a perturbation responsible for the ramp rate limitation causes the effective ramp rate limitation loss, and it is reasonable to expect this loss to depend on the transverse resistance between strands. The relationship between Q_{errl} and the transverse resistance may not be a simple one, however. It is possible that the transverse resistivity is not constant, but depends on the deformation at each strand-to-strand interface. The deformation may be caused by the local stresses in the cable as a result of the local Lorentz forces, and hence the transport current and magnetic field. Furthermore, it may not be possible to predict the transverse resistivity based on these factors alone: the chemical makeup of the strands' surfaces may significantly alter the contact resistance from magnet to magnet and over time.

In addition, any stability model accounting for the current diffusion during and after a ramp rate limitation perturbation must necessarily include the thermal resistance to heat flow at the contact points between strands. This thermal resistance may depend

on the surface area of the contact points, which is subject to deformation by the Lorentz forces as well. Unfortunately, no such stability model currently exists.

One way to investigate the effect of transverse resistance may be to perform ramp rate tests on CIC magnets made from identical wire and with all other parameters equal except with differing insulating thicknesses on the strands. The AC losses may be computed and measured (as in Chapter 2), and the energy margin computed by computer and measured (as in Chapter 3). Assuming the Q_{other} value in Eq. 5.4 to be small, the value of Q_{err} may be determined by subtracting the AC losses from the energy margin value at the quench current. In this way, an empirical relationship for Q_{err} may be made and plotted simultaneously with $Q_{AC\ loss}$ as a function of ramp rate and transverse resistivity (such as in Fig. 5.1). The results from such a measurement would indicate the highest attainable quench current possible for a given ramp rate and transverse resistivity, manifesting which transverse resistivity yields the largest stability margin for a given ramp rate design value.

5.1.4 Controlling Effective Transverse Resistance

The effective transverse resistance between strands depends on the resistivity of the insulating layer coated on the surface of the strands, on the contact resistance at the interface between copper and insulation, and on the contact resistance at the interface between two strands. Some results have shown that the contact resistance may be a significant contribution to the net resistance between two conductors, and hence control of the contact resistance becomes important in implementing step (5) in the plan (in Section 5.1). Whereas determination of the resistivity of the insulation (chromium, for example) is relatively simple, calculating the value of the contact resistance is not. A study by Ciazynski and Turck (1994) proposed a model to calculate the contact resistance that was subsequently shown by experiment to give errors in the contact resistance value on the order of 10^3 . To date, no theory to adequately determine the resistance contribution at the strand interface to the total transverse resistance has been forthcoming.

In order for knowledge of the optimum effective transverse resistivity to be useful for the magnet designer, he must be able to prescribe *a priori* the parameters that produce

the desired effect. It has been proposed that the contact resistance be at least partly determined by the contact area between the strands, subject to deformation due to changing stresses during ramp. If this be the case, the material selected for the strand insulation plays a role in determining contact resistance due to its mechanical properties; however, the thickness of the insulating layer may also play a role. For this reason, it is proposed that an experiment be performed to investigate the dependence of insulation thickness on the total transverse resistance. Using the same identical samples—except with differing insulation thicknesses—as the experiment proposed in section 5.1.3, a four lead technique to measure the resistance distributed along the length of a pair of strands could be employed. Each different pair of strands would be tested; then other cables with different insulation thicknesses would be tested. The measured resistance would be attributed to the net transverse resistivity between the pair of strands and correlated to the insulation thickness. Modification of this proposal could then be made to include the effects of the Lorentz forces. With the resistivity of the insulation assumed to remain constant, any changes in resistance between strands must be due to the change in contact resistance. If successful, the magnet designer could then prescribe the optimum transverse resistivity for a ramping magnet.

5.2 Conclusion

The discovery of a serious degradation in magnet performance at high ramp rates, known as a ramp rate limitation, jeopardizes the success of superconducting CIC magnets for use as the poloidal pulse coils in a tokamak reactor. To date, no ramp rate limitation has been observed to cause a magnet to quench at currents lower than the traditionally-defined limiting current; nevertheless, the stability of a magnet under transient conditions may be decreased below the traditional stability margin because of the ramp rate regardless of the proposed maximum operating current. During a ramp, when AC losses and the phenomenon responsible for the ramp rate limitation are activated, the magnet has its greatest susceptibility to quenching due to anomalous or otherwise intractable disturbances. Consequently, a magnet must be designed to have the highest stability margin possible during the ramping period to ensure robustness.

It has been proposed that the transverse resistivity plays a role in determining the stability margin during ramping periods. The widely accepted theory of AC losses indicates that the larger the effective transverse resistivity, the smaller the energy dissipated by coupling currents between strands. One extreme criterion for acceptable AC losses at the design stage is AC losses must be at least below the minimum energy required to initiate a magnet quench. Because the transverse resistivity between strands depends in part on the insulation coating the strands' surface, the thicker the insulating layer the smaller the AC losses, and hence the larger the stability margin.

It has been further proposed that the transverse resistivity plays a role in the ramp rate limitation. An experiment to determine the functional dependence of the thickness of the strand coating on the effective ramp rate limitation loss has been proposed. The success of the experiment depends on considering the source of AC losses and the ramp rate limitation as uncoupled phenomenon. This is reasonable if the maldistribution of current among the strands is responsible for the ramp rate limitation and if the traditional stability theory is valid during a current (or field) ramp, because the traditional stability theory calculates the energy margin by assuming that each strand carries the same current. The proposed experiment determines the current at which a magnet will quench with both AC losses and the ramp rate limitation present, from which the AC losses contribution to the quench energy may be subtracted. In the absence of a suitable stability theory for ramping magnets that takes into account the ramp rate limitation phenomenon, the results of the experiment can then be used to determine the effective transverse resistance that maximizes the quench current for any given ramp rate. This effective resistance will therefore provide the largest stability margin for the designed ramp rate, regardless of the designed maximum operating current.

Finally, an experiment to determine the functional relationship between strand coating thickness, stress due to Lorentz forces, and the total resistance between strands (including contact resistance) is proposed. The results of this and the previous experiment would allow magnet designers to select the optimum value of insulating thickness in order to maximize the stability of the magnet for the proposed operating environment. In addition, the experiment may provide insights that will lead to an understanding of the

phenomenon responsible for the ramp rate limitation, and ultimately to a new stability theory for magnets under transient conditions.

The opportunity to increase the stability of a superconducting magnet against an undesirable quench is of paramount importance to the success of tokamak machines and other magnets as well. Indeed, since all magnets—even DC magnets—must be subjected to transient conditions at some point, increasing the stability margin advances the technology of superconducting CIC poloidal coil magnets for the ITER in specific, and of all superconducting magnets in general.

BIBLIOGRAPHY

- Amemiya, N. and O. Tsukamoto. (1994) "Stability Analysis of Multi-strand Superconducting Cables." Presented at the Applied Superconductivity Conference (ASC): Boston, Massachusetts, October 16-21.
- Ando, T. *et. al.* (1988) "Design of the Nb₃Sn Demo Poloidal Coil (DPC-EX)." *IEEE Transactions on Magnetics*: vol. 24, no. 2 (March), pp. 1444-1447.
- Armstrong, J. (1992) "Experimental Investigation of Cooling Perimeter and Disturbance Length Effect on Stability of Nb₃Sn Cable-in-Conduit Conductors." Japan Atomic Energy Research Institute: JAERI-M 92-013.
- Bottura, L. (1994) "Limiting Current and Stability of Cable-in-conduit Conductors." *Cryogenics*: vol. 34, no. 10, pp. 787-794.
- Ciazynski, D. *et. al.* (1993) "AC Losses and Current Distribution in 40-kA NbTi and Nb₃Sn Conductors for NET/ITER." *IEEE Transactions on Applied Superconductivity*: vol. 3, no. 1 (March), pp. 817-824.
- Ciazynski, D. and B. Turck. (1993) "Stability Criteria and Critical Energy in Superconducting Cable-in-Conduit Conductors." *Cryogenics*: vol. 33, no. 11, pp. 1066-1071.
- Ferri, Matthew A. (1994) "Current Distribution in Cable-in-conduit Superconductors." S.M. Thesis, Department of Nuclear Engineering, Massachusetts Institute of Technology. (unpublished)
- Isono, T. *et. al.* (1993) "Development of Full-scale Conductors for the ITER Central Solenoid Scalable Model Coils." Presented at the 13th International Conference on Magnet Technology: Victoria, B.C., Canada, September 20-24.
- Iwasa, Yukikazu. (1994) *Case Studies in Superconducting Magnets: Design and Operational Issues*. Plenum Press: New York, New York.
- Jeong, S. *et. al.* (1994) "Ramp-Rate Limitation Test of Cable-In-Conduit Conductors at Supercritical Helium." Presented at the Applied Superconductivity Conference (ASC): Boston, Massachusetts, October 16-21.

- Koizumi, N. *et. al.* (1994) "Experimental Results on Instability Caused by a Non-uniform Current Distribution in the 30kA-NbTi Demo Poloidal Coil (DPC-U) Conductor." *Cryogenics*: vol. 34, no. 2, pp. 155-162.
- Lue, J. W. (1994) "Review of Stability Experiments on Cable-in-conduit Conductors." *Cryogenics*: vol. 34, no. 10, pp. 779-786.
- "Magnet Design Criterion for the ITER CS Coil" (1994) Document from ITER workshop, dated June 6. (unpublished)
- Miller, J. R. (1985) "Empirical Investigation of Factors Affecting the Stability of Cable-in-conduit Superconductors." *Cryogenics*: vol. 25 (October), pp. 552-557.
- Morgan, G. H. (1970) "Theoretical Behavior of Twisted Multicore Superconducting Wire in Time-varying Uniform Magnetic Field." *Journal of Applied Physics*: vol. 41, no. 9, pp. 3673-3679.
- Nelson, Richard J. *et. al.* (1993) "An Investigation of A.C. Losses in Two Sub-size Conductors for the ITER." Japan Atomic Energy Research Institute: JAERI-M 93-219.
- Nelson, Richard J. (1994) "Initial Results of Coupling Time Constant in a Sub-Size Sample with 4 μm Chromium Insulation." Research In Progress at the Japan Atomic Energy Research Institute. (Unpublished)
- Nishi, M. *et. al.* (1993) "Ramp-Rate Limitation Test Results of the Nb₃Sn Demo Poloidal Coil (DPC-EX)." Presented at the 15th Symposium on Fusion Engineering: Hyannis, Massachusetts, October 11-15.
- Orlando, Terry P. and Kevin A. Delin. (1991) *Foundations of Applied Superconductivity*. Addison-Wesley: Reading, Massachusetts.
- Painter, T. *et. al.* (1992) "Test Data from the US-Demonstration Poloidal Coil Experiment." MIT Plasma Fusion Center: Cambridge, Massachusetts.
- Takahashi, Y. *et. al.* (1991) "Experimental Results of the Nb₃Sn Demo Poloidal Coil (DPC-EX)." *Cryogenics*: vol. 31 (July), pp. 640-644.

- Takayasu, M. *et. al.* (1993) "Measurements of Ramp-rate Limitation of Cable-in-conduit Conductors." *IEEE Transactions on Applied Superconductivity*: vol. 3, no. 1 (part 2) (March), pp. 456-459.
- Turck, B. (1974) "Influence of a Transverse Conductance on Current Sharing in a Two-layer Superconducting Cable." *Cryogenics*: vol. 14 (August), pp. 448-454.
- Turck, B. (1992) "Transverse Resistance in Conduit Conductors: AC Losses Versus Current Transfer." Presented at the Applied Superconductivity Conference (ASC): Chicago, Illinois, August 23-28.
- Wilson, Martin N. (1983) *Superconducting Magnets*. Clarendon Press: Oxford, U.K.
- Yamaguchi, M. *et. al.* (1985) "Stability Analysis Code ALEPH II for Forced-cooled Superconducting Coils." Japan Atomic Energy Research Institute: JAERI-M 85-108.